Correspondence to:

A. Kehm,
alexander.kehm@tum.de

Combination Strategy for the Geocentric Realization of Regional Epoch Reference Frames

A. Kehm[1] , L. Sánchez[1], M. Bloßfeld[1], M. Seitz[1] , H. Drewes[1], D. Angermann[1], and F. Seitz[1]

[1]Deutsches Geodätisches Forschungsinstitut (DGFI-TUM), Technical University of Munich, Munich, Germany

Abstract For high-resolution regional geodetic applications, the International Terrestrial Reference Frame (ITRF) is complemented by regional densifications. These are realized either as multi-year solutions related to a tectonic plate (e.g., EUREF for Europe) or as epoch reference frames (ERFs) to capture nonlinear geophysical station motions caused by, for example, earthquakes or non-tidal loading (e.g., SIRGAS for Latin America). These Global Navigation Satellite Systems (GNSS)-only based regional reference frames have in common that their geodetic datum is aligned with the ITRF datum at a specific epoch. The consequence is that their origin represents the Earth's center of figure and does not coincide with the instantaneous center of mass. Here, we present studies on a direct geocentric realization of regional ERFs. We propose to realize the geodetic datum for each epoch by combining global GNSS, Satellite Laser Ranging, and Very Long Baseline Interferometry networks via measured local ties at co-located sites. A uniformly distributed global GNSS network is used to realize the orientation via a no-net-rotation constraint with respect to the ITRF and is densified by the stations of the regional subnetwork. The developed combination and filtering strategy aims to guarantee a stable datum realization for each epoch-wise solution. Validating our results against global reference frames and geophysical loading models relating to the Earth's centers of mass and figure, we show that the realized displacement time series are geocentric and reflect seasonal geophysical processes. As the approach does not need to rely on co-location sites in the region of interest, it is conceptually transferable to other regions on the globe.

Plain Language Summary In today's world, precise ground, sea, and air navigation and the accurate monitoring of geophysical processes are vital. Precise coordinate reference frames make it possible to relate observed displacements to the Earth system. For different regions, these reference frames are materialized by dense networks of Global Navigation Satellite Systems (GNSS) stations with precisely determined position coordinates. It is crucial that the origin (defined to coincide with the Earth's center of mass), the scale (the realized unit of length), and the orientation (with respect to the Earth's crust) of the reference frame match their conventional definition. The realization of this so-called "geodetic datum" for current conventional reference frames suffers from several deficiencies. We have developed a strategy for the precise weekly geocentric realization of regional reference frames. Coping with the changing and inhomogeneous distribution of stations by observing different space-geodetic techniques, we developed and implemented a strategy to improve the long-term stability of the solutions. We show that this approach allows for monitoring geophysical processes (loading and earthquakes) at low latency and overcomes the problems of existing realizations. The developed strategy is based on global networks and its effectiveness is demonstrated in Latin America; however, it can be applied to any region of the Earth.

1. Introduction

Geodetic reference frames do not only provide the basis for surveying, mapping, or space-based positioning and navigation, but they are also the foundation for the reliable localization and quantification of changes in the Earth system (Plag & Pearlman, 2009). Continuous geodetic monitoring of the Earth's surface geometry, gravity field, and orientation in space has enabled the precise determination of long-term and transient surface deformations and mass redistributions in the Earth's interior and its environment, including the oceans, atmosphere, hydrosphere, and cryosphere. Measurements, data processing, and estimated parameters must be related to a common and consistent reference frame to determine global change effects reliably. The International Terrestrial Reference System (ITRS; Petit & Luzum, 2010) is the global basis for the determination of coordinates on the Earth's surface or in its near environment and for the establishment of regional dense reference networks. Realizations of the ITRS are provided in the form of the International Terrestrial Reference Frame (ITRF; Petit & Luzum, 2010).

ITRF solutions are based on the combination of observation time series of four space-geodetic techniques: Very Long Baseline Interferometry (VLBI), Satellite Laser Ranging (SLR), Global Navigation Satellite Systems (GNSS), and Doppler Orbitography and Radiopositioning Integrated by Satellite (DORIS). Each technique contributes to the realization of the reference system with particular strengths: the coordinate origin, which is defined to coincide with the center of mass (CM) of the Earth system—that includes solid Earth, oceans, hydrosphere, cryosphere, and atmosphere—, is realized from SLR observations only. This is because SLR observations are most sensitive to the Earth's gravity field and less dependent on modeling uncertainties that are inherent to GNSS and DORIS. The scale is realized from the weighted average of the VLBI and SLR scale information. GNSS and DORIS improve the station distribution worldwide. In addition, GNSS significantly contributes to the realization of the orientation of the reference frame with respect to the Earth's surface due to the globally well-distributed station network. For recent ITRF solutions, the orientation is realized by the constraint of a no-net-rotation (NNR) to maintain the orientation of the new solution in accordance with its predecessor (Altamimi et al., 2016). The observation data from the global space-geodetic networks are preprocessed and provided by Scientific Services of the International Association of Geodesy (IAG), namely the International VLBI Service for Geodesy and Astrometry (IVS; Nothnagel et al., 2017) for VLBI, the International Laser Ranging Service (ILRS; Pearlman et al., 2019) for SLR, the International GNSS Service (IGS; Johnston et al., 2017) for GNSS, and the International DORIS Service (IDS; Willis et al., 2015) for DORIS.

According to the conventions of the International Earth Rotation and Reference Systems Service (IERS; Petit & Luzum, 2010), an ITRF solution is provided by a set of mean station positions referring to a specific epoch and linear position changes over time (station velocities) that permit to infer coordinates at any time for all the stations considered in the computation. The linear parametrization of the station positions results in an ITRF origin that reflects the CM only in a mean sense, meaning on secular time scales.

Geophysical events (such as earthquakes) and instrumental updates induce changes in station positions or velocities. To take into account these effects as well as changes in the observing networks, it is necessary to recompute the ITRF coordinates regularly. Thus, ITRF solutions are released in intervals of several years, because the linearly extrapolated coordinates become too inaccurate for many applications. This also holds for the realized datum parameters. Recent ITRF releases also benefit from the increased accuracy of the contributions from the individual techniques as longer observation time series and improved background models are used in the data processing. The ITRF version in use at the time of this study is the ITRF2014 (Altamimi et al., 2016), provided by the Institut national de l'information géographique et forestrière (IGN). The ITRF2014 is combined from technique-specific solutions provided by the IAG Scientific Services and provides linear station motions that have been determined after applying a priori models for post-seismic trajectories. The latter have been approximated by logarithmic or exponential functions at stations affected by earthquakes. Besides the ITRF2014, two independent solutions are provided, which are used for validation and quality assurance of the solution: These are the DTRF2014 (M. Seitz et al., 2022) provided by the Deutsches Geodätisches Forschungsinstitut at the Technical University of Munich (DGFI-TUM), and the JTRF2014 (Abbondanza et al., 2017) provided by the NASA Jet Propulsion Laboratory (JPL). The former, like the ITRF2014, is a conventional secular multi-year reference frame solution, but is based on the combination of datum-free technique-specific normal equations (instead of solutions), while the latter is a sub-secular epoch-wise geocentric realization of the ITRS based on Kalman filtering over the observation period. The advantages of the different approaches are that the conventional secular realizations ITRF2014 and DTRF2014 relate to a secular CM and can be extrapolated linearly beyond the observation period, while the origin of the JTRF2014 relates to an instantaneous CM within the observation period. The solutions are about to be replaced by the 2020 realizations of the ITRS, which will cover a longer observation time span and improved modeling. Thereby, the JTRF2020 will switch from a Kalman filtering approach, combined and filtered at the level of solutions, to an information filtering approach developed for combination and filtering at the level of normal equations (Chin, 2020).

Common to all three aforementioned ITRF solutions is that the computational effort to process multiple decades of input data restricts these global reference frames to a limited subset of the stations that are actually available. Hence, regional reference frames are necessary to ensure close-by accessibility to the global reference frame. In particular, GNSS users require reference stations near their areas of interest, while the ITRF station distribution is not dense enough for many applications. Therefore, regional reference frames are primarily realized as densifications of the ITRF through GNSS station networks, the technique used for most

geodetic applications since it is cheaper and easier to handle than VLBI, SLR, or DORIS. Regional reference frames are either realized as multi-year solutions related to a continental plate (e.g., the European Reference Frame EUREF/ETRS89; Altamimi, 2018) or as epoch reference frames (ERFs) to capture geophysical effects like earthquakes or loading displacements (e.g., the Sistema de Referencia Geodésico para las Américas SIRGAS; Sánchez et al., 2016). Their consistency with the ITRF is achieved by aligning the regional network via NNR, no-net-translation (NNT), or no-net-scale (NNS) constraints over either a regional or a global subset of common stations, so-called fiducial stations. For station displacements in regional ERFs on seasonal and short time scales, the alignment of networks to the ITRF datum means that their origin reflects the geometric center of the Earth, often called the center of figure (CF), rather than the CM (Dong et al., 2003). As we focus on the interpretation of seasonal effects, hereafter, we denote displacement time series that relate to an instantaneously realized CM as "CM-related" and displacement time series in a frame aligned to the ITRF datum as "CF-related."

The two principal consequences of the usage of linearly modeled fiducial coordinates are:

1. Mass variations in the atmosphere, the hydrology, and the ocean lead to a relative variation between the CM and the CF (materialized by the stations of the reference frame), an effect often referred to as "geocenter motion" (e.g., Collilieux & Altamimi, 2009; Collilieux et al., 2009). Consequently, the reference frame is moving with respect to the (geophysical) geocenter (Drewes et al., 2013), meaning that the derived coordinates are inappropriate for a direct geophysical interpretation of environmental effects like loading-induced site displacements. The effects of this disagreement must be considered if the regional reference frame coordinates shall be assimilated into CM-frame-based geophysical models.

2. Seismic events may cause considerable deformations, resulting in abrupt changes of point coordinates as well as changing station velocities in an extended area. As an example, Figure 1 shows the station velocity changes at selected reference stations in Latin America induced by strong earthquakes since 2010. As the traditional multi-year reference frames provide station positions at a reference epoch and constant velocities derived from a limited data period, there is no reliable reference frame in these regions after earthquakes that occur in the extrapolation period of the reference frame (i.e., after the last observation epoch considered during its computation). By nature, this effect is inherent to all low-latency or real-time applications. A geocentric reference frame should thus be computed at short time intervals to overcome this deficiency and to ensure a reliable basis for the operational activities based on GNSS positioning. This also holds for any other nonlinear effects like monument motion, antenna replacements, or anthropogenic changes that may result in continuously changing point coordinates that the linear velocity model cannot fully describe.
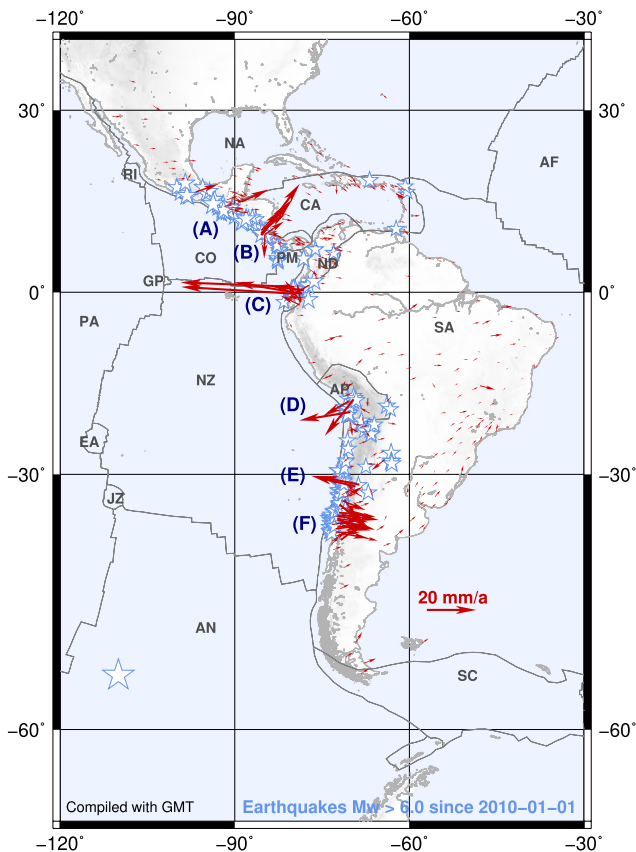
Figure 1. Changes in the Latin American reference frame kinematics induced by strong earthquakes. They are inferred from the difference between the two latest multi-year solutions SIR15P01 (Sánchez & Drewes, 2016) and SIR17P01 (Sánchez & Drewes, 2020). Blue stars represent earthquakes with Mw > 6.0 since January 1, 2010. The large discrepancies appear close to the epicenter of strong earthquakes: (A) Guatemala (Mw: 7.4, 2012-11-11), (B) Nicoya (Mw: 7.6, 2012-09-05), (C) Pedernales (Mw: 7.8, 2016-04-16), (D) Iquique (Mw: 8.2, 2014-04-01), (E) Illapel (Mw: 8.3, 2015-09-16), and (F) El Maule (Mw: 8.8, 2010-02-27).

The disadvantage of the alignment to linearly parametrized reference coordinates is that neither seasonal variations, for example, caused by atmospheric, oceanic, and hydrological loading (Seitz & Krügel, 2009; F. Seitz et al., 2014; Glomsda, Bloßfeld, et al., 2021), nor anthropogenic changes such as subsidence due to groundwater withdrawal (e.g., Bevis et al., 2005), are fully modeled in the reference coordinates. Moreover, especially in the extrapolation period of a reference frame, episodic changes like seismic events (Sánchez & Drewes, 2016, 2020) are no longer represented in the reference coordinates. The accuracy of the geocentricity of the resulting coordinates thus decreases over time, meaning that the coordinates' information value for research of geodynamics or global change decreases substantially.

Gómez et al. (2022) show that the consistency between the ITRF and regional densifications aligned to the ITRF datum can be significantly increased by adding periodic displacement information to the ITRF station motion model. Thereby, the regional reference frame inherits the ITRF datum by equalizing the station trajectory models in both the ITRF and the regional reference frame. However, this approach relies on the availability of reference positions over time; meaning that outside the time span covered by the ITRF, still extrapolation is needed and the accuracy of the datum inherited from the ITRF decreases.

Within this study, we develop an alternative methodology to compute regional ERFs that shall be realized epoch-wise for short periods to cover non-linear station motions, that shall be geocentric at any epoch to relate these motions directly to geophysical phenomena, and that shall ensure the stability of the realized physical datum parameters origin and scale over time. We propose to realize the datum of the regional ERFs directly by combining GNSS with SLR and VLBI data, omitting the realization of the origin and the scale by the usual alignment to a multi-year reference frame via fiducial points. The orientation is realized by a non-deforming NNR constraint with respect to the ITRF2014 over a global GNSS network (Drewes, 2009). As the approach shall be suitable to provide solutions at short latencies, the datum of the regional reference frame shall be realized from the most recent observation data.

A major issue of geodetic datum parameters realized from SLR and VLBI for short observation periods is that they suffer from an inhomogeneous station distribution and permanently changing observation network geometries, the so-called "network effect" (Collilieux et al., 2009). Based on DGFI-TUM's approach to realize the datum of geodetic reference frames by combining the space-geodetic techniques at the normal equation level (e.g., Angermann et al., 2004; M. Seitz et al., 2012, 2022) comparisons between previous DTRF multi-year reference frames and epoch-wise independent realizations of the ITRS from short observation periods revealed that a sophisticated treatment of the network effect is required to realize reliable non-linear station displacement time series (Bloßfeld et al., 2014), whereby the reliability of the resulting datum parameters and the temporal resolution of the epoch-wise solutions are in an inverse relationship (Bloßfeld et al., 2015).

To solve the issue, we propose to filter the SLR and VLBI information before the combination. The methodology shall be suitable to realize a series of ERFs with reliable geocentric station coordinates in near real-time at all epochs, also after sudden changes like earthquakes. Furthermore, the resulting station coordinate time series shall be qualified to serve as a basis for the direct interpretation of station displacements in terms of geophysical processes.

We evaluate the developed methodology based on the Latin American network covered by SIRGAS. The SIRGAS network, located in one of the world's most seismically active regions, is affected by frequent strong earthquakes. In addition, an important number of stations are in the Amazon region, where seasonal variations in the time series may reach the decimeter level due to surface and ground water changes. Thus, Latin America presents the ideal conditions to demonstrate the feasibility of a realization of regional geocentric ERFs. Comparing the solutions with the ITRF2014, the JTRF2014, as well as geophysical models of site displacements, we can point out the benefits and remaining deficiencies of our approach.

Within this study, we compute two solutions for geocentric weekly ERFs: an unfiltered (U-ERF) and a filtered ERF solution (F-ERF). The filter is applied at the normal equation level to the SLR and VLBI networks before the inter-technique combination to reduce datum deficiencies related to station performances and varying network geometries. A reprocessed SIRGAS-like solution (SIRGAS-repro) aligned to the ITRF2014 datum via fiducial points is used for validation. The two following sections outline our starting point based on the Latin American region (Section 2) and the general concepts on which our new approach is based (Section 3). Section 4 describes the input data and the preprocessing steps. The developed combination and filtering strategies are provided in Section 5. The validation of the results is discussed in Section 6, whereby our solutions are compared against each other and the external references. A concluding summary and final discussions are provided in Section 7.
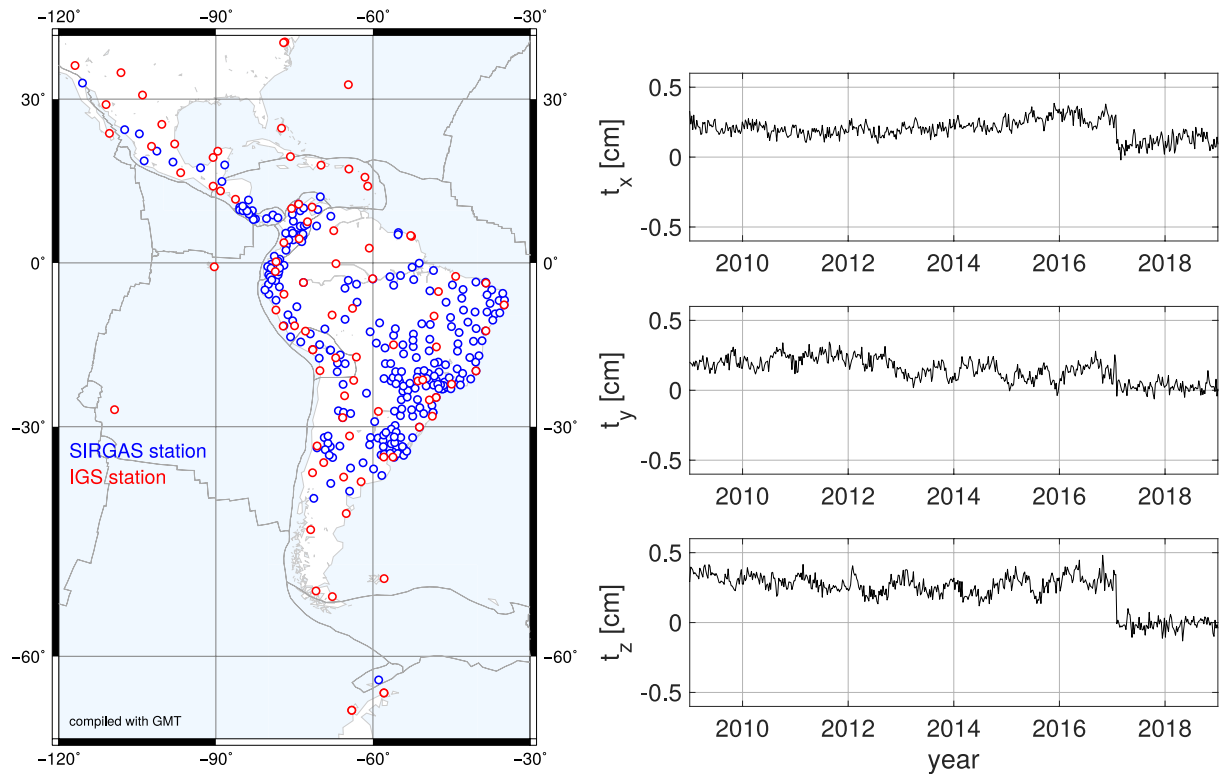
Figure 2. SIRGAS reference frame network (left) and translations of the SIRGAS/IGS weekly solution with respect to ITRF2014 (right). The translations have been determined via a seven-parameter similarity transformation of the global network of IGS core stations.

2. SIRGAS Reference Frame and Geodynamics in Latin America

SIRGAS is the regional densification of the ITRF in Latin America (Brunini et al., 2012; Drewes et al., 2005; Sánchez et al., 2013, 2016; SIRGAS, 1997). Currently, it is composed of about 400 continuously operating GNSS stations (Figure 2, left panel). About 70 of these stations are included in the IGS global network (Johnston et al., 2017). The SIRGAS data processing strategy follows the IERS conventions (Petit & Luzum, 2010) and the IGS's most recent GNSS processing guidelines (Johnston et al., 2017). The only exception is that the GNSS satellite orbits and clock offsets as well as the Earth orientation parameters (EOPs) are not estimated within the SIRGAS processing but fixed to their weekly final IGS values (Johnston et al., 2017). Further details about the SIRGAS processing strategy are provided by Brunini et al. (2012), Sánchez et al. (2016), and Sánchez and Drewes (2016).

The operational SIRGAS products are provided in weekly ERF solutions for station positions. The datum of a weekly operational SIRGAS solution (cf. Figure 4, left column) is inherited from the respective IGS weekly solution via a 1 mm constraint over a regional subnet of common stations, the SIRGAS core stations (Sánchez et al., 2022; Sánchez & Kehm, 2021). The datum of the IGS weekly solution itself is aligned to the IGS reference frame via a global set of fiducial points that are extrapolated with linear coordinate changes, meaning constant station velocities, from the reference epoch to the corresponding epoch (Rebischung et al., 2016).

An IGS reference frame is a selection of ITRF positions and velocities for a set of suitable GNSS stations, which are used as fiducial points for the generation of the IGS satellite orbits, satellite clock offsets, and EOPs, as well as the corrections for the phase center variations at both transmitting and receiving antennas. For instance, the IGS14/IGb14 reference frame (Rebischung, 2020; Rebischung et al., 2016; Rebischung & Schmid, 2016) corresponds to the ITRF2014 (Altamimi et al., 2016). As there is no translation, rotation, or scale difference between both reference frames (ITRF and IGS), the IGS final products and the computations based on them are considered in the corresponding ITRF datum (Kouba, 2009). Since the SIRGAS data analysis is based on the IGS reference frame valid when the GNSS data are routinely processed, the operational SIRGAS normal equations are

given in different reference frames (details given in Sánchez & Kehm, 2021; Sánchez et al., 2022). Reprocessing campaigns of the historical data are regularly undertaken (Sánchez et al., 2016) to ensure consistency among the complete SIRGAS observation time series since 2000. A reprocessed series of solutions (here referred to as SIRGAS-repro) has been computed according to the most recent standards to avoid the impact of changes in the SIRGAS operational processing strategy and background models. It is constrained to the most recent series of IGS weekly solutions.

Due to the frequent occurrence of seismic events in the western margin of Latin America, the concept of conventional position/velocity solutions poses a practical problem. For instance, strong earthquakes result in global and regional reference frame solutions becoming inconsistent and the datum realization via fiducial coordinates not being reliable anymore. In addition to linear plate motion effects, time series of GNSS station positions show significant non-linear variations attributed to seismic events, post-seismic deformation, or seasonal non-tidal loading (NT-L) effects (mainly in the vertical component), but they actually reflect a combined effect of non-modeled geophysical effects and uncertainties associated to the GNSS observations or GNSS data analysis (e.g., Blewitt et al., 2001; Collilieux et al., 2010, 2012; Drewes et al., 2013; Ray et al., 2008; Zou et al., 2014). These effects lead to a seasonal motion of the entire IGS weekly/SIRGAS network with respect to the ITRF2014 origin (Figure 2, right panel). The step visible in the translation time series is related to the switch of the applied models for antenna phase center variation (PCV) from igs08.atx to igs14.atx in January 2017; see Rebischung et al. (2016). Therefore, one main challenge is to assess how much of the detected motion of a site is attributable to the uncertainties associated with the datum realization and data processing, and how much is caused by mass variations or geophysical effects.

Figure 3 displays the SIRGAS-repro time series of four stations located close to the Equator and to Antarctica, respectively. The two stations in far southern geographic latitudes (RIO2 and PALM) are affected by seasonal motions of similar amplitude in the North (N) component, albeit located on two different tectonic plates. In theory, one would expect these motions to be referable to NT-L displacements in a CF-frame (as the SIRGAS datum is aligned to the linear ITRF2014 origin). Projecting the translation time series of the SIRGAS-repro solution with respect to the ITRF2014 origin into each station's local level system reveals that systematic variations in the realized origin directly map into the differences between modeled NT-L and measured site displacements. These systematic variations add up with geophysically induced motions. Similar common behavior is visible for two stations in the Amazon basin (BELE and NAUS). In the equatorial region, the step induced by the switch in PCV models in 2017 is mapped into the N and East (E) components. We can thus conclude that the SIRGAS origin, as currently realized, is not geocentric, neither in an instantaneous sense (CM-related) nor strictly in a mean sense (CF-related for seasonal changes). The first is expected as the datum is aligned to the multi-year linear ITRF2014 datum via an NNT constraint, the second can be related to unmodeled fiducial point displacements or changes in background models that lead to a common motion of the whole reference frame. This common motion directly maps into the derived station position time series.

3. Concept for a Direct Geocentric Realization

Depending on the focus of interest, there are two possible ways of realizing the datum of regional ERFs: The first would be to maintain the strategy as it is but improve the datum realization via fiducial coordinates for a more accurate alignment with the ITRF2014 datum. By these means, one could stick to the concept of processing GNSS-only solutions, but consequently, coordinate variations would still be CF-related, meaning that the CM-minus-CF content of NT-L signals would still be missing in the station-specific displacement time series, as it is removed by the application of NNT constraints with respect to the ITRF2014. This would allow for a direct interpretation with respect to geophysics only after a correction of the CM-minus-CF variation from external geophysical models.

Because of the growing interest in exploiting geodetic data for geophysical investigations, the second possibility would be a direct epoch-wise geocentric realization of the datum of the ERFs, resulting in CM-related coordinates at each epoch. This would imply the processing not only of a globally extended GNSS network but also of global SLR and VLBI networks. The great advantage of such a solution would be the direct interpretability of station displacement time series in a geophysical sense, without having to rely on external information on the motion of a multi-year reference frame with respect to the geocenter. By these means, geodetic observations could contribute
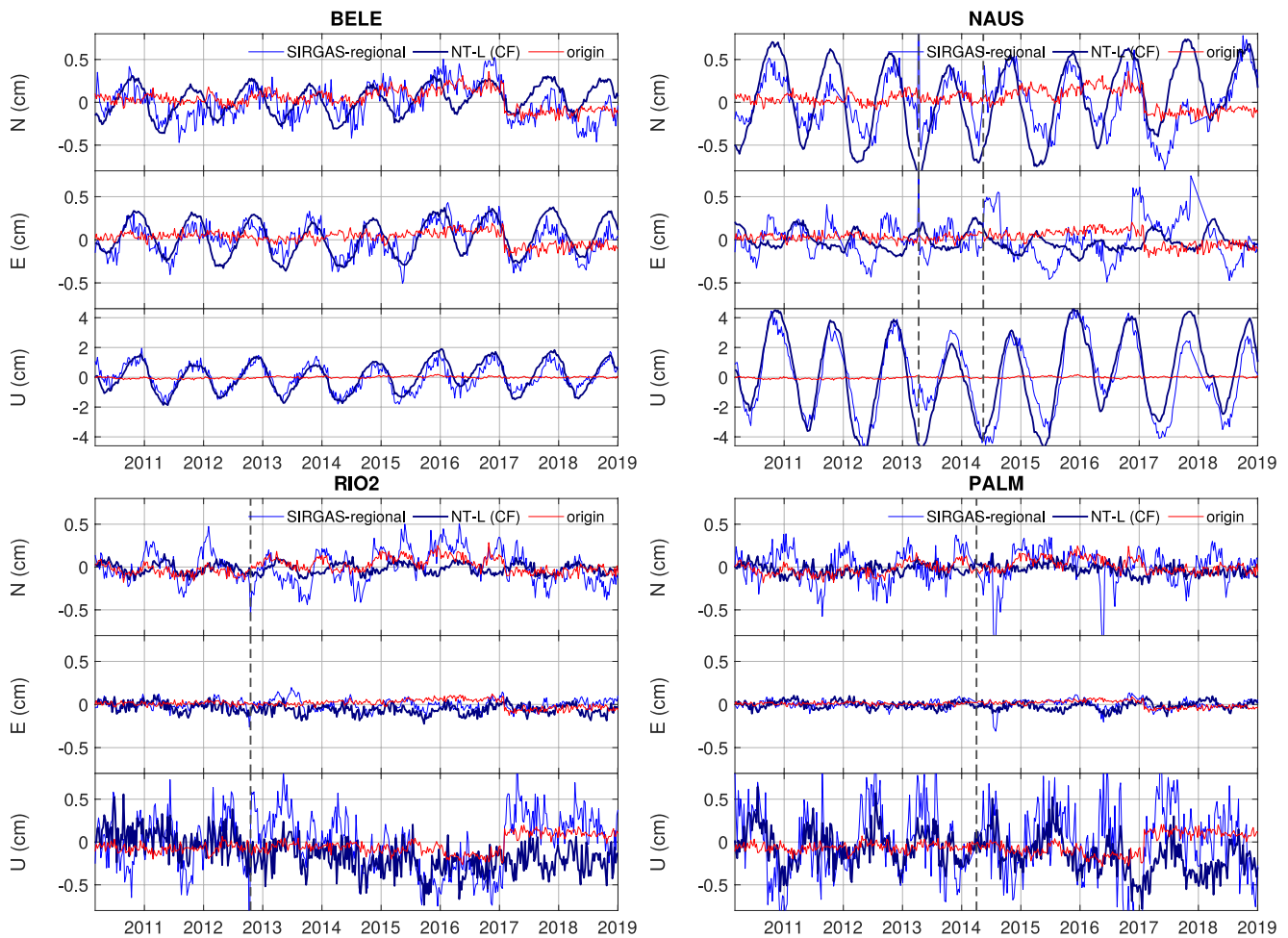
Figure 3. SIRGAS-repro coordinate time series of stations BELE (Belém, Brazil; top left), NAUS (Manaus, Brazil; top right)—both located in the Amazon basin—, RIO2 (Río Grande, Argentina; bottom left) located in Tierra del Fuego and PALM (Palmer) located in Antarctica compared to the ESMGFZ NT-L time series (Dill & Dobslaw, 2013) in CF-frame. The red graph in each plot represents the variation of the SIRGAS origin with respect to the ITRF2014 origin (cf. Figure 2, right panel), mapped into each station's local level system. A common disagreement with the NT-L time series is visible in the N and Up (U) components for RIO2 and PALM. This disagreement corresponds to the variation of the SIRGAS origin mapped into the stations' local level systems. Another common pattern is visible in the N and E components of the Amazon basin stations. Dashed vertical lines denote jumps removed from the position time series.

directly to interpreting geophysical processes and the improvement and validation of geophysical models. Within this study, we investigate the second approach and have developed a strategy for a direct realization of the datum of weekly regional geocentric ERF solutions based on the reference frame for Latin America.

Major outcome of this study is series of ERF solutions for Latin America, whereby the datum of each epoch-wise solution shall be consistent with the ITRS. The datum realization is performed by combining the three space-geodetic techniques SLR, VLBI, and GNSS. The origin is realized by SLR—the only technique permitting its realization with highest accuracy—, and the scale is realized as a weighted mean by SLR and VLBI. Because these two techniques are responsible for the physically defined datum parameters (in contrast to the orientation, which is defined by a mathematical constraint), we later denote these techniques as the "datum-relevant techniques." The solution is computed with minimum datum constraints to keep the geocentricity of the ERF. The orientation is realized via an NNR constraint over the global GNSS (IGS stations) network (Figure 4). The datum transfer between the techniques is performed by introducing local ties at co-located sites, which are locally measured difference vectors (ties) between the technique-specific reference points at sites equipped with more than one of the space-geodetic techniques used. Because, in our case, the target parameters are the positions of the GNSS stations contained in the regional network covered by SIRGAS, we do not include DORIS in the combination as this technique serves to densify the global ITRF2014 station network (cf. Section 1) though it does not yet contribute to the datum parameters origin and scale.
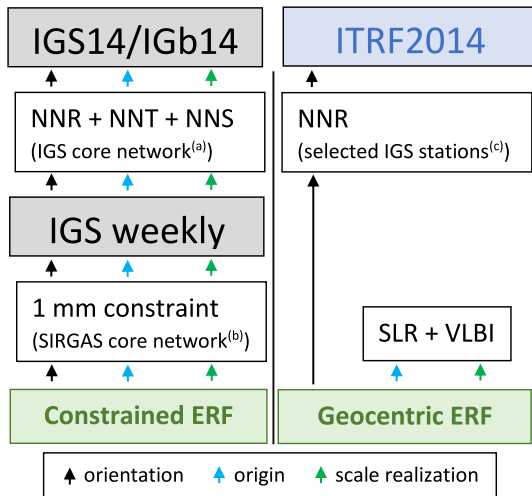
Figure 4. Concepts of datum realization for the SIRGAS regional ERFs (left) and a direct geocentric realization of ERFs (right). (a) cf. Rebischung et al. (2016); (b) cf. Sánchez and Kehm (2021); (c) cf. Section 4.1. The colors of the arrows refer to the different datum parameters. The datum of the IGS14/IGb14 and the ITRF2014 reference frames is considered identical.

As our approach shall be suitable to compute ERF solutions that are short-term realizations of the ITRS relying on the most recent observation data, a treatment of the network effect, meaning apparent variations in the observed origin and scale caused by variations in the observing networks, is of special importance. Both SLR and VLBI suffer from sparse and inhomogeneous network distributions. As demonstrated in various simulation studies (e.g., Glaser et al., 2017; Glaser, König, Neumayer, Balidakis, et al., 2019; Glaser, König, Neumayer, Nilsson, et al., 2019; Kehm et al., 2018, 2019; Otsubo et al., 2016; Pavlis & Kuźmicz-Cieślak, 2009), a substantial extension of the global SLR and VLBI networks would significantly stabilize the datum parameters realized.

However, for the time being, we must deal with the existing networks and their apparent variations, often caused by observational gaps of individual stations. Consequently, it is necessary that stations provide a sufficient number of observations for a reliable position estimation. The selection of stations included in the normal equations (NEQs) is thereby a part of the technique-specific preprocessing done by the providers of the NEQs, namely the Analysis Centers of the technique-specific IAG Scientific Services and the regional network Analysis Centers. In the case of the SLR reprocessing done specifically for this study, these standards are chosen in accordance with those applied by DGFI-TUM within its involvement as an ILRS Analysis Center (cf. Section 4.2). Table 1 gives an overview of the gaps within the station time series of VLBI and SLR stations. As can be seen, approximately 50% of the gaps extend over one week whereas about 10% of the gaps extend over more than 8 weeks. Another approximately 10% of the gaps have a length of between 4 and 8 weeks. To increase the stability of the networks, one major point of our study has thus been to investigate the way in which a filtering approach allows sufficient bridging of these observational gaps to reduce the network effect, without systematically distorting the datum parameters realized (cf. Section 5.2).

4. Space-Geodetic Input Data

4.1. Reprocessing SIRGAS Normal Equations for Combination With SLR and VLBI

An appropriate combination of global SLR, VLBI, and GNSS networks is required to implement an epoch-wise datum realization for regional networks. In our case, the regional GNSS network must be extended beyond the area covered by the SIRGAS network to include SLR/GNSS and VLBI/GNSS co-located stations and enough GNSS stations to realize the orientation via an NNR constraint. Therefore, one main objective of the study was to identify the GNSS network configuration required for a reliable datum realization. Different scenarios were evaluated in this context. The first considered only those GNSS sites co-located with SLR and VLBI (blue circles and green dots in Figure 5). As most of these stations are in the northern hemisphere, this station distribution did not turn out to be favorable for the GNSS data preprocessing. Consequently, additional GNSS sites have been included to ensure a more homogeneous global network distribution, which is also favorable for a reliable realization of the orientation. After a series of empirical experiments, our main conclusion is to include the core stations of the IGS14/IGb14 reference frame into the GNSS data processing.

Further research concentrated on the simultaneous determination of GNSS satellite orbits, satellite clock offsets, EOPs, and station positions within the GNSS data processing. Although we use a global network in the computations, simultaneous inclusion of all SIRGAS regional stations reduces the reliability of the EOPs and GNSS orbits due to the dense station distribution in one specific region (see Figure 5). Therefore, we

Table 1

Ratio of Gaps ≥1 Week in Station Time Series of Very Long Baseline Interferometry (VLBI) and Satellite Laser Ranging (SLR) Stations Between 2000 and 2014

Gap length	SLR	VLBI
1 week	50.0%	46.7%
2 weeks	17.4%	16.5%
3 weeks	8.6%	10.3%
4 weeks	4.5%	5.7%
5–8 weeks	8.5%	11.7%
>8 weeks	11.0%	9.1%

Note. Corresponding to our combination approach, the investigation is based on GPS weeks.
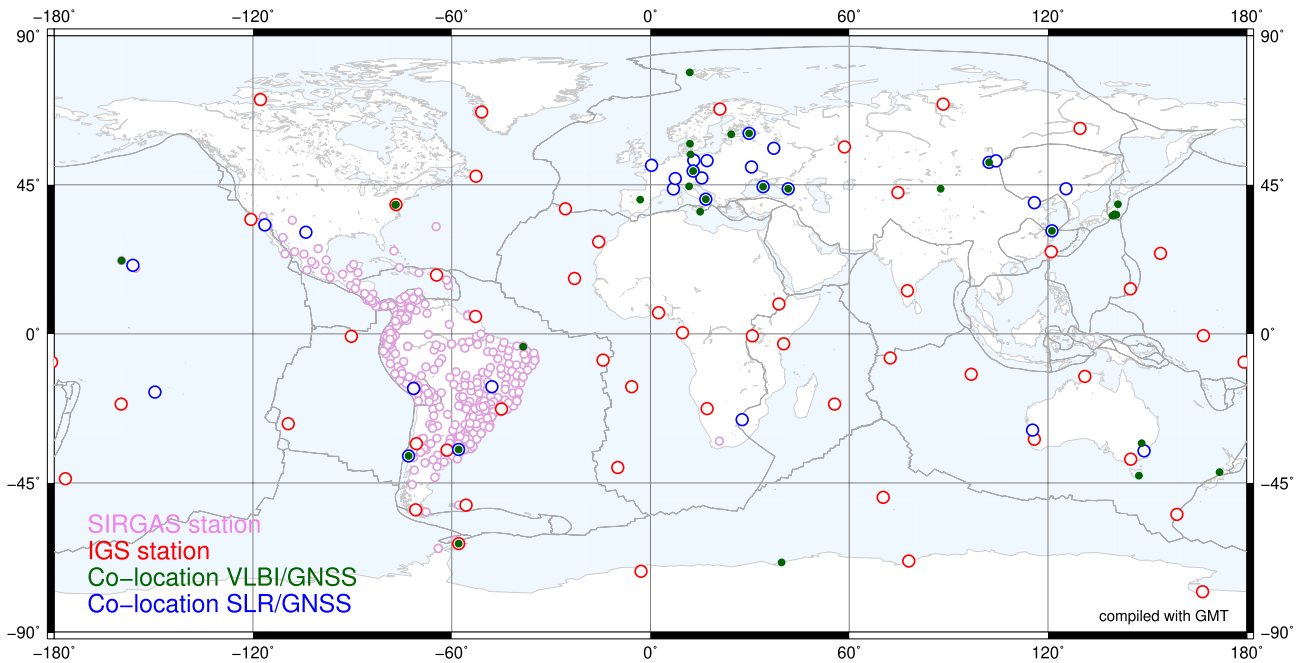
Figure 5. Extension of the SIRGAS network to enable its combination with VLBI and SLR as well as the realization of the orientation via an NNR constraint.

apply a two-step procedure: (a) orbit and EOP determination based on the IGS global reference frame network, and (b) processing of the GNSS data (global + regionally densified network), whereby the previously determined orbits and EOPs are fixed. A priori datum information introduced into the GNSS NEQs by fixing the orbits and the EOPs is removed before combining them with the SLR and VLBI NEQs. This is performed by introducing and reducing (pre-eliminating) seven Helmert parameters (three translations, three rotations, and one scale parameter; cf. Bloßfeld, 2015). Thus, the GNSS NEQs introduced into the combination process are free from datum information.

The SIRGAS data reprocessing for this study covers January 2000 to December 2020. It is based on the IGS14/IGb14 reference frame and includes 530 SIRGAS and 135 IGS reference stations (30 co-located with SLR and 31 co-located with VLBI). This reprocessed global GNSS network is called the SIRGAS extended network hereafter. The GNSS data processing was carried out with the Bernese GNSS software Version 5.2 (Dach et al., 2015); the resulting weekly NEQs for combination are provided in the Solution INdependent EXchange Version 2.02 (SINEX v2.02) format (cf. IERS Message No. 103, 2006).

4.2. Satellite Laser Ranging and Very Long Baseline Interferometry

Besides a full reprocessing of the SIRGAS GNSS network, the SLR and VLBI input data also underwent a full reprocessing to comply with the most recent standards and conventions (Petit & Luzum, 2010, including updates until v 1.3.0).

For SLR, we performed reprocessing specifically for this study. We extended the current standard four-satellite-constellation processed by DGFI-TUM in its function as an ILRS Analysis Center (AC; Bloßfeld & Kehm, 2020), namely LAGEOS-1/2 (LAser GEOdynamics Satellite-1/2) and Etalon-1/2, by a fifth satellite, LARES (LAser RElativity Satellite). This is planned to be the future ILRS standard setup to ensure a higher stability of the SLR-derived origin (Bloßfeld et al., 2018). The satellites have been combined into weekly NEQs applying a variance component estimation (VCE) as described by Bloßfeld (2015). Satellite-specific parameters and orbits have been prereduced from the NEQs, leaving station positions and range biases as explicit parameters. Aligned to the standards of the ILRS routine processing, a station's observations to all five satellites are considered in a weekly NEQ only if at least 10 observations and two passes have been observed for at least one of the satellites LAGEOS-1, or LAGEOS-2, or LARES.

Table 2
Input Data to the ERF Combination

Technique	Temporal resolution	Processing setup	Datum constraints
		SINEX NEQ content	
SLR	Weekly	Future ILRS 5-satellite setup	No
		Station coordinates	
		Range biases	
		EOPs	
VLBI	Session-wise	CORE/NEOS/R1/R4 sessions	No
		station coordinates	
		Source coordinates	
		EOPs	
GNSS	Weekly	SIRGAS + global IGS network	Yes (to be removed)
		Station coordinates	

For VLBI, we rely on the VLBI contribution of DGFI-TUM to ITRF2020 (Glomsda et al., 2020). This data set has no NT-L correction applied and is thus consistent with the routine processing standards of the other techniques. This contrasts with DGFI-TUM's routine contribution within its function as an IVS Analysis Center, "dgf2020a," which contains a priori corrections for non-tidal atmospheric loading (Glomsda, Seitz, et al., 2021). We use the twice-weekly CORE/NEOS (until 2001) and R1/R4 (from 2002 on) sessions, as these are available on a permanent twice-weekly basis and contain sufficient co-location sites for datum realization. VLBI-specific parameters like troposphere and clock are prereduced and thus not explicitly contained in the NEQs. The properties of all technique-specific contributions are summarized in Table 2.

The SLR and VLBI NEQs are free from datum constraints and thus only contain the datum information to which the respective observations are sensitive. The SLR and VLBI data processing was carried out with the Orbit Computation (-OC) and Radio Interferometry (-RI) branches of the DGFI Orbit and Geodetic parameter estimation Software (DOGS; Bloßfeld, 2015; Gerstl, 1997; Kwak et al., 2017), respectively. The resulting weekly (SLR) or session-wise (VLBI) NEQs for combination are provided in the SINEX v2.02 format.

5. Combination Strategy

5.1. General Approach

This section is dedicated to describing the basic concept of the combination approach. The inter-technique combination is performed at the NEQ level (implementation at DGFI-TUM described in detail by Bloßfeld, 2015) with the DOGS-CS Combination and Solution library (Gerstl et al., 2008). The combination at the NEQ level has the advantage that it avoids the inconsistencies caused by independently constrained technique-specific solutions (e.g., M. Seitz et al., 2015). Station positions are estimated within a least-squares adjustment according to the Gauß-Markov model (Gauss, 1823; Koch, 2004).

Each NEQ system is set up by

$$\mathbf{N}d\hat{\mathbf{x}} = \mathbf{y},$$ (1)

consisting of the NEQ matrix $\mathbf{N}$, the vector of estimated parameters $d\hat{\mathbf{x}}$ and the right-hand side of the equation system $\mathbf{y}$. The system is solved for $d\hat{\mathbf{x}}$ by multiplication with the cofactor matrix of the estimated parameters

$$\mathbf{Q}_{d\hat{\mathbf{x}}} = \mathbf{N}^{-1},$$ (2)

and additionally yields the a posteriori variance factor

$$\hat{\sigma}_0^2 = \frac{\mathbf{v}^{\mathrm{T}}\mathbf{P}\mathbf{v}}{n - u}.$$ (3)
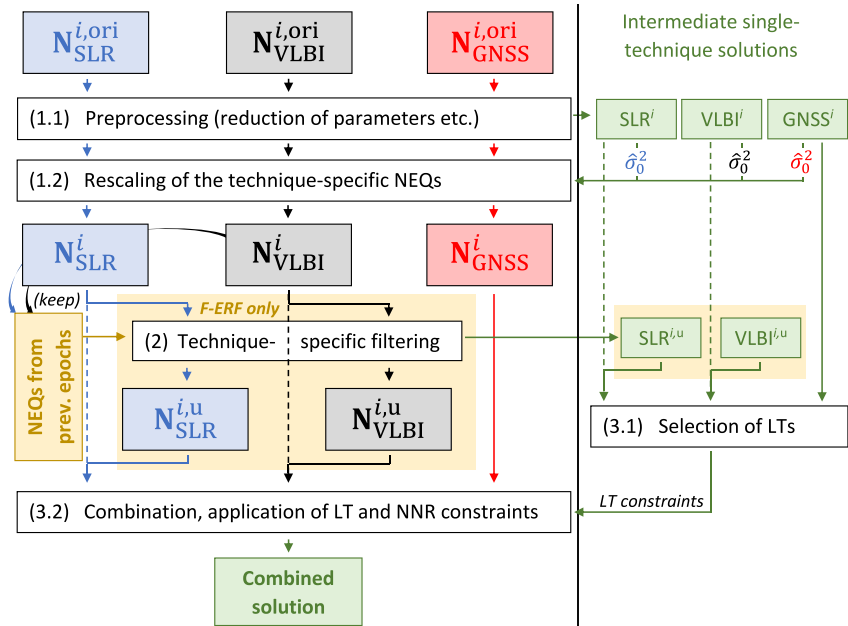
Figure 6. Concept of technique-specific filtering (SLR and VLBI) and inter-technique combination for epoch t_i. Dashed lines denote the unfiltered processing chain (U-ERF); light yellow boxes contain the additional steps performed only within the filtered processing chain (F-ERF).

Here, $\mathbf{v}$ is the vector of observation residuals, n is the number of observations, and u is the number of unknowns.

In the standard case of the Gauß-Markov model, $\hat{\sigma}_0^2$ serves to check whether the stochastic and functional models chosen a priori are consistent with the observations. If the latter is the case and if the a priori variance factor had been chosen as 1.0, then $\hat{\sigma}_0^2$ should also be close to 1.0. In this case:

$$\Sigma_{\mathbf{d\hat{x}}} = \mathbf{Q}_{\mathbf{d\hat{x}}}, \tag{4}$$

with $\Sigma_{\mathbf{d\hat{x}}}$ being the variance-covariance matrix of the estimated parameters.

Weekly NEQs $\left(\mathbf{N}_{\text{tech}}^i\right)$ from SLR and GNSS and session-wise NEQs from VLBI are the input data for the combination. The processing for an epoch t_i comprises the following steps (Figure 6):

1. Prehandling the technique-specific NEQs. Calculation of intermediate single-technique (U-ST; "U" stands for "unfiltered") solutions.
2. Rescaling of the technique-specific NEQs with their respective a posteriori variance factors from the U-ST solutions.
3. Filtering the SLR and VLBI NEQs (F-ERF solution only). Calculation of intermediate filtered single-technique (F-ST) solutions.
4. Local tie selection and weighting procedure based on the single-technique solutions.
5. Inter-technique combination, the introduction of local tie and NNR constraints, and the subsequent solution of the combined NEQ.

In Step 1, incoming single-technique NEQs $\mathbf{N}_{\text{tech}}^{i,\text{ori}}$ are prepared for the combination. This includes accumulating the sessions of a week into one common NEQ for VLBI, reducing EOPs for SLR and VLBI, reducing range bias parameters for SLR, and eliminating source coordinates, in other words, fixing the celestial reference frame (CRF), for VLBI. The datum information from the GNSS NEQs is removed as described in Section 4. As a result, each NEQ is free from artificial datum information and only contains station coordinates as explicitly estimated parameters. Afterward, the intermediate U-ST solution is calculated with minimal constraints (i.e., NNR for SLR, NNR + NNT for VLBI, and NNR + NNT + NNS for GNSS). The system is solved according to Equations 1 and 2. The derived a posteriori variance factor $\hat{\sigma}_0^2$ (Equation 3) is used to rescale the NEQ in Step 2. The U-ST

solutions will be used for the local tie selection and weighting procedure performed in Step 4. Moreover, they are used to validate the datum realization (cf. Section 6).

Step 2 performs the rescaling of the NEQ with its reciprocal a posteriori variance factor $1/\hat{\sigma}_0^2$ to fulfill Equation 4. The resulting prehandled and rescaled technique-specific NEQ $\mathbf{N}_{\text{tech}}^i$ will be the actual input to the subsequent filtering and combination steps.

Step 3 performs the filtering for SLR and VLBI (F-ERF solution only): The single-technique NEQs are filtered by weighted accumulation over a limited number of weeks before the combination (cf. Section 5.2) to guarantee an enhanced stability of the physically derived datum parameters origin and scale. The outcome is a NEQ $\mathbf{N}_{\text{tech}}^{i,\text{u}}$ (where "u" stands for "updated") for this week, which is later used for the combination. Afterward, the intermediate F-ST solution is calculated with minimal constraints. The SLR and VLBI F-ST solutions are introduced into the local tie selection and weighting procedure performed in Step 4.

Step 4 performs the local tie selection and weighting procedure (cf. Section 5.4). For the U-ERF solution, we use the GNSS solution and the U-ST solutions of SLR and VLBI from Step 1, while for the F-ERF solution, we use the GNSS solution from Step 1 and the F-ST solutions of SLR and VLBI from Step 3. The outcome is a set of local tie constraint equations introduced into the combination and solution procedure performed in Step 5.

Step 5 performs the actual inter-technique combination. The technique-specific NEQs are combined into one NEQ

$$\mathbf{N}_{\text{comb}}^i = \lambda_{\text{SLR}} \cdot \mathbf{N}_{\text{SLR}}^{i,\text{u}} + \lambda_{\text{VLBI}} \cdot \mathbf{N}_{\text{VLBI}}^{i,\text{u}} + \lambda_{\text{GNSS}} \cdot \mathbf{N}_{\text{GNSS}}^i, \tag{5}$$

applying the technique-specific relative weights λ_{tech} (cf. Section 5.3). After introducing the local tie constraint equations set up in Step 4 and adding an NNR constraint over a global selection of IGS stations (cf. Section 4.1), the solution is computed from the combined NEQ $\mathbf{N}_{\text{comb}}^i$ according to Equations 1 and 2.

5.2. Filtering

Our approach is based on the concepts developed by Bloßfeld et al. (2014, 2015), whereby the epoch-wise independently realized geodetic datum parameters shall be stabilized by an appropriate filtering. As all combination steps are performed at the NEQ level, we implement an information filtering approach, a transfer of the Kalman filter (Kalman, 1960) approach from the solution level to the NEQ level (e.g., Assimakis et al., 2012; Chin, 2001). The approach enables us to apply relevant modifications directly to the NEQ systems without a need to solve the system beforehand. The filter generally implements a kinematic model that predicts displacements of the stations within the network and a stochastic model that predicts the evolution of their accuracy, or, in other words, the reliability of the predicted state.

As SLR and VLBI are the critical techniques for realizing the physically defined datum parameters for the regional GNSS network, their availability for each weekly ERF solution is crucial. Thereby, a network geometry that is as stable as possible must be achieved to minimize the network effect on the datum parameters realized. The developed filtering strategy needs to be compromised between

1. the optimal filling of observational gaps for single stations and
2. the fact that the physical relevance of observations for the instantaneous datum realization is only given for a limited time span.

The information of interest from the NEQs of the datum-relevant techniques SLR and VLBI is exclusively the implicitly contained datum information. This information is provided by the observing networks as a whole, and single stations at co-location sites serve to transfer the datum information to the GNSS network within the combined solution. As our goal is short-term realizations of the ITRS derived from recent observation data, we are not interested in modeling motions of individual non-observing stations over long periods. The artificial information thereby introduced (based on assumptions) would potentially distort the realized datum. The contribution of a single station to the datum realization shall be based solely on its observations; consequently, our chosen kinematic filter model assumes positions of individual stations to be constant for a certain period (up to a few weeks) without observations. Our filter's prediction step is thus intended to modify the stochastic information
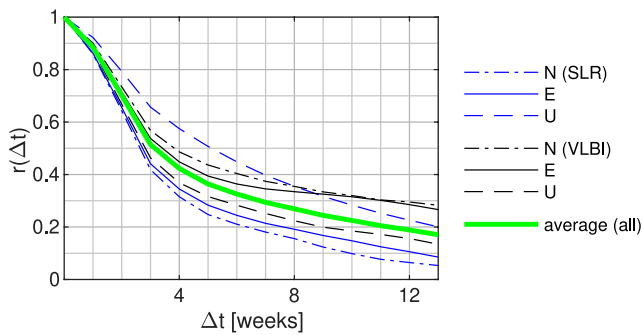
Figure 7. Average auto-correlation behavior of selected SLR and VLBI site displacement time series.

contained in the NEQ so that the decreasing reliability of the datum information due to unknown displacements is considered.

As a result of the considerations described above, we realize the prediction step by consistently modifying the complete stochastic information contained in the NEQ. Thereby, the prediction of a NEQ $\mathbf{N}_{tech}^{i-1}$ from epoch t_{i-1} to a NEQ $\mathbf{N}_{tech}^{i,p}$ at epoch t_i is performed by rescaling the NEQ with a factor $\kappa \in [0, 1]$:

$$\mathbf{N}_{tech}^{i,p} = \kappa \cdot \mathbf{N}_{tech}^{i-1} \tag{6}$$

Afterward, the update step is performed, resulting in an updated NEQ

$$\mathbf{N}_{tech}^{i,u} = \begin{cases} \mathbf{N}_{tech}^{i,p} + \mathbf{N}_{tech}^{i} & \dots \text{ if } \mathbf{N}_{tech}^{i} \text{ exists,} \\ \mathbf{N}_{tech}^{i,p} & \dots \text{ otherwise,} \end{cases} \tag{7}$$

with $\mathbf{N}_{tech}^{i}$ being the incoming information update for epoch t_i. Usually, an information update for SLR and VLBI is available every week (especially in our reprocessing scenario), so the second case is mainly relevant for rare occasions of processing delays in the routine processing.

Because of the above requirement 2, we choose to filter the information from a specific epoch only over a limited period of $w + 1$ weeks into the future (i.e., for all further prediction steps, the weighting factor κ is 0). Consequently, the filtered NEQ of epoch t_i is equal to a weighted sum of the NEQs from epoch t_{i-w} to epoch t_i. Each summand is only present if an NEQ for the respective epoch exists:

$$\mathbf{N}_{tech}^{i,u} = \sum_{n=0}^{w} \kappa^n \cdot \mathbf{N}_{tech}^{i-n} \tag{8}$$

The two filter parameters to be set are the filter weight κ to be applied within each prediction step and the "cutoff" number of prediction steps w after which the weight of an NEQ is set to 0.

For the determination of κ, auto-correlation functions have been computed for several stations that observed continuously for multiple years and have not been affected by earthquakes. These functions follow a common pattern for both SLR and VLBI in all three coordinate components. This lets us compute an average auto-correlation function that roughly follows an exponential pattern for the first couple of weeks (Figure 7). For both SLR and VLBI, the average auto-correlation $r(\Delta t)$ of the station position time series decreases weekly to about 0.5 after 3 weeks. From this, we deduce an approximate decrease factor of 0.8 per week. Introducing this into Equation 6 as a rescaling factor $\kappa = 0.8$ means that the overall variance level of an NEQ is raised by a factor of $1/\kappa$ per prediction step, increasing the standard deviations for non-observing stations by about 12%.

The cutoff number of prediction steps w has been chosen after 3 weeks (each prediction step is equivalent to a step of 1 week), meaning that a station will be present in the solution for no more than 3 weeks after its last observation. Concerning the above requirement 1, this yields approximately 75% of the observational gaps within both the SLR and VLBI time series being bridged, leaving only the remaining 25% of gaps that are longer than 3 weeks (cf. Section 3, Table 1). In this way, we significantly reduce the network effect (cf. Section 6.1). The cutoff prediction step yields a downweighting of the respective NEQ to a factor of $\kappa^3 = 0.51$ by applying the rescaling factor of $\kappa = 0.8$. The resulting standard deviations are scaled by a factor of 1.4 for stations that did not provide an observation update after this epoch.

5.3. Technique-Specific Weights

It is well known that the standard deviations of GNSS estimates are too optimistic due to neglected correlations in the stochastic modeling implemented in the processing software (Schön & Brunner, 2008; Schön & Kutterer, 2007). This means that, although internally fulfilling the condition formulated in Equation 4, the relative weight of the GNSS NEQ is too high compared to SLR and VLBI and could systematically distort the combined solution while simultaneously yielding too accurate standard deviations. Therefore, technique-specific

Table 3

Ratio Between Average Estimated Standard Deviations and Empirically Derived WRMS Values (3D Station Coordinates; Upper Line) and Technique-Specific Weights Applied Within the Combination (Lower Line)

	SLR	VLBI	GNSS
$WRMS/\sigma$	1.3 ± 0.2	1.1 ± 0.3	9.7 ± 3.1
Weight applied	1.0	1.0	0.01

a priori weights are determined by calculating the ratio between an empirically derived weighted root mean square (WRMS) deviation and the average formal error (estimated standard deviation) of several representative and continuous coordinate time series. Thereby, the WRMS has been calculated from the time series content that can be considered noise rather than signal. The noise part of the time series has been extracted by applying a bandpass filter that sets the amplitudes of all periods above a threshold of 13 weeks (a quarter year) to 0, leaving only the short periods below the threshold. The coordinate time series have been chosen from stations that do not show significant peaks in the coordinate spectra for periods below the threshold. Table 3 gives the empirically derived ratios between estimated standard deviations and the WRMS of the three-dimensional (3D) coordinate time series. The resulting ratio between WRMS and formal error is close to 1 for SLR and VLBI, while it is close to 10 for GNSS. Consequently, the GNSS NEQs are introduced into the combination with an a priori scaling factor of $\lambda_{GNSS} = 0.01$ while the scaling factor for SLR and VLBI is set up to $\lambda_{SLR} = \lambda_{VLBI} = 1.0$.

5.4. Treatment of Local Ties

The datum transfer between the different techniques is performed by introducing measured local ties as constraints. Thereby, the global set of IGS GNSS sites included in the SIRGAS extended network ensures that all available co-locations between GNSS, SLR, and VLBI can be exploited.

In this study, the local tie treatment is based on the procedure described in detail by M. Seitz et al. (2012). The basis is the local tie table initially compiled to realize the DTRF2014 (M. Seitz et al., 2022). Concerning the techniques combined here, the table contains local ties for 95 inter-technique station pairs (49 GNSS-SLR pairs, 38 GNSS-VLBI pairs, and 8 SLR-VLBI pairs) and 24 intra-technique station pairs (15 GNSS-GNSS pairs, 6 SLR-SLR pairs, and 3 VLBI-VLBI pairs). Here, multiple measurements of the same local tie are counted only once. The local tie selection and weighting are performed independently for each epoch-wise ERF solution. The local tie constraints are selected and weighted according to the discrepancy between the measured local tie and the coordinate difference derived from the single-technique solutions. In the process, only local ties below a certain discrepancy threshold are considered. For the U-ERF solution, this threshold is chosen as 50 mm to achieve enough local ties per week (38 on average). A larger threshold of 70 mm would not yield a significant increase in the number of available local ties, but experiments showed that solutions might suffer from the introduction of single local ties which do not fit the local situation. This effect becomes worse when the threshold is further increased. For the F-ERF solution, the threshold for local tie introduction can be tightened to a discrepancy of 30 mm (cf. Table 4). Additional stations from the filtering enable the use of more local ties which fulfill a stricter discrepancy criterion. This yields a more stable datum realization in the F-ERF solution than U-ERF solution (cf. Section 6.1).

To avoid systematic network deformations, some local ties must be excluded, especially at those stations affected by severe earthquakes (Table 5). This is necessary because local ties might still pass the selection procedure despite small systematic errors. As a result, we consider it necessary to remeasure the local ties at affected stations after major seismic events.

6. Results and Validation

6.1. Datum Realization

This section presents the validation of the datum realization of our approach, whereby we perform a two-step procedure: First, the impact of combination and filtering on the realized datum parameters is investigated to confirm the non-introduction of systematic deficiencies and the benefits from filtering. This is done by comparing the datum-relevant single-technique solutions, the F-ERF, and the U-ERF solutions against each other and against the

Table 4

Average Weekly Number of Local Ties Selected for the U-ERF and F-ERF Solutions, Respectively, Depending on the Discrepancy Criterion

Solution	Discrepancy criterion	GNSS-SLR	GNSS-VLBI	SLR-VLBI	Intra-tech.	Total
	30 mm	14.0	9.6	1.5	8.6	33.7
U-ERF	**50 mm**	16.4	11.0	1.8	8.7	37.9
	70 mm	17.1	11.3	1.9	8.7	39.0
	20 mm	14.0	11.5	2.2	7.4	35.1
F-ERF	**30 mm**	18.1	13.9	2.8	8.7	43.5
	50 mm	20.3	15.6	3.0	8.8	47.7

Note. The criterion selected for combination is marked bold.

Table 5
Sites Co-Located With GNSS With Local Ties Excluded After Major Seismic Events

Site	DOMES no.	Technique	From	Event
Concepción	41719M001	SLR	2010-02-27	Maule Earthquake
Concepción	41719S001	VLBI	2010-02-27	Maule Earthquake
Monument Peak	40497M001	SLR	2010-04-04	El Mayor-Cucapah Earthquake
Tsukuba	21730S007	VLBI	2011-03-11	Tōhoku Earthquake
Arequipa	42202M003	SLR	2017-07-18	Peru Earthquake

ITRF2014 in terms of Helmert transformation parameters. Afterward, the quality of the epoch-wise instantaneous datum realization of our solution is evaluated by validating the F-ERF solution against the JTRF2014.

Table 6 summarizes the impact of combination and filtering on the single-technique and combined solutions. Table 7 summarizes the weighted mean and RMS deviations along the transformation time series of the U-ST and F-ST solutions of VLBI and SLR, respectively, with respect to the ITRF2014; shown are the non-constrained datum parameters. Table 8 presents the weighted mean and RMS values along the transformation time series of the technique-specific subnetworks of the U-ERF and F-ERF solutions with respect to the ITRF2014.

For the U-ERF solution, we can state that the datum realization via the introduced local ties has no systematic effects on the datum-relevant technique-specific subnetworks. The comparison between the SLR U-ST solution and the combined U-ERF solution shows no significant impact on the SLR origin and scale; the same holds for the VLBI-derived scale (Table 6, U-ERF w.r.t. U-ST). The comparison of the solutions with respect to the ITRF2014 (Figure 8; Table 7, U-ST; Table 8, U-ERF) confirms that the transfer of the origin from SLR to the VLBI and GNSS networks is well-performed, although with a systematic effect of about -3.5 mm in t_z for GNSS. A drift is observed in the scales of SLR and VLBI after 2015, the end of the observation period of the ITRF2014. The scale of the GNSS subnetwork lies between the scales from SLR and VLBI. This confirms that the scale of the GNSS subnetwork is realized as a weighted mean of the SLR and VLBI scales.

For the F-ERF solution, we can state that filtering the datum-relevant techniques SLR and VLBI has no systematic effects on the realized datum parameters. The comparison between the U-ST and the F-ST solutions of SLR and VLBI shows no systematic impact on the subnetworks (Table 6, F-ST w.r.t. U-ST). The same holds for the combination step following filtering, which is seen by a comparison between the F-ERF and the F-ST solutions (Table 6, F-ERF w.r.t. F-ST). This confirms that the networks are not deformed by the selected local ties (all mean values are below ± 0.1 mm for the SLR origin and scale and -0.04 mm for the VLBI scale).

While the general behavior of both the F-ERF and the U-ERF solutions is identical (Figures 8 and 9), a significant decrease in the WRMS of the transformation parameters with respect to the ITRF2014 is observed for the F-ERF solution compared to the U-ERF solution (Table 8). This is mostly due to a reduced noise of these time series which is caused by the increased network stability achieved in the F-ERF solution by closing observational gaps. A periodic variation is expected as each ERF solution is realized in an instantaneous CM-frame, whereas the ITRF2014 is a long-term CM-frame. It is important to note that the F-ERF solution also shows a reduction

Table 6
Impact of Filtering and Combination on the Datum Parameters Derived by SLR and VLBI in Terms of Helmert Parameters Between the Solutions

Technique	Datum parameter	U-ERF w.r.t. U-ST		F-ST w.r.t. U-ST		F-ERF w.r.t. F-ST	
		Mean [mm]	RMS [mm]	Mean [mm]	RMS [mm]	Mean [mm]	RMS [mm]
SLR	t_x	−0.1	0.6	0.3	2.4	0.0	0.3
	t_y	−0.1	0.5	−0.1	2.0	−0.1	0.3
	t_z	−0.4	1.2	−0.3	4.8	−0.3	0.5
	scale	0.2	0.5	−0.1	1.6	0.1	0.2
VLBI	*scale*	−1.1	2.2	0.0	2.9	−0.7	1.1

Table 7
Datum Parameters of the Single-Technique Solutions With Respect to ITRF2014

Technique	Datum parameter	U-ST		F-ST		Δ [%]
		Wmean [mm]	WRMS [mm]	Wmean [mm]	WRMS [mm]	
SLR	t_x	−1.6	4.4	−0.9	3.5	−20
	t_y	0.0	3.6	−0.4	2.8	−22
	t_z	2.2	7.7	1.6	5.7	−25
	scale	1.5	3.5	1.4	2.8	−18
VLBI	*scale*	4.8	4.6	4.7	3.1	−31

of the systematic offsets compared to the U-ERF solution, especially for t_z. For the GNSS network, the relative offset to the SLR origin is reduced from −3.5 to −2.8 mm. This might be related to the better distribution and a larger number of available local ties per week achieved by filtering. The frequency spectra (Figure 10) of the translations of the SLR solutions (U-ST and F-ST with respect to the ITRF2014), the SLR subnetwork of the F-ERF solution, and the GNSS subnetwork of the F-ERF solution agree in the main frequencies with a decrease in the amplitude of the annual period translation for GNSS compared to SLR. This damping may be related to the large and more homogeneously distributed global network (compared to SLR).

To validate the geocentricity of the solutions, we also compare our results with the JTRF2014, which is a sub-secular geocentric realization of the ITRS based on Kalman filtering (Abbondanza et al., 2017, 2020). In addition to the transformation parameters of the U-ERF and F-ERF solutions, Figures 8 and 9 present the time series of the Helmert parameters between JTRF2014 and ITRF2014. Figure 10 shows the respective spectra. As can be seen, the amplitudes of the annual period signals are damped for the F-ERF solution compared to the JTRF2014, which holds predominantly for t_x and t_y. This can most probably be related to the fact that these periods are explicitly modeled in the JTRF2014 (Abbondanza et al., 2017). The results of a direct transformation between the F-ERF solution and the JTRF2014 are given in Table 9. Figure 11 depicts the corresponding spectra of the translation and scale difference time series.

The WRMS differences between the F-ERF solution and the JTRF2014 are in the range of 3 mm for t_x and t_y and 4.6 mm for t_z. The systematic offsets are in the range of ≤1 mm. The spectra (Figure 11, upper panel) do not contain dominant peaks for t_x and t_y, which holds also for the semi-annual and annual periods. For t_z, an amplitude of approximately 1.5 mm is visible near the annual band but not dominant in the spectrum. The scale offset of 1.8 mm is probably caused by the different correction models used for the antenna phase center variations. While the JTRF2014 (like ITRF2014 and DTRF2014) is consistent with the igs08.atx model, the reprocessed GNSS NEQs used in our study are based on the igs14.atx model (more details in Rebischung et al., 2016). Apart from the offset, the scale of the F-ERF solution does not show systematic variations with respect to JTRF2014 (Figure 11, lower panel).

We conclude that the datum parameters realized for the F-ERF solution correspond with the geocentric datum of the JTRF2014 without significant systematic differences in their time evolution.

6.2. Interpretation of the Results With Respect to Geophysical Processes

In this section, we compare the F-ERF solution with loading models to quantify how well geophysical processes are represented in the time series. Our validation is based on geophysical fluid loading site displacement models (Dill & Dobslaw, 2013) provided by the Earth System Modeling group (ESMGFZ) of the Deutsches Geoforschungszentrum (GFZ) Potsdam. We use the sum of three NT-L components, namely non-tidal atmospheric (NTAL), non-tidal oceanic (NTOL), and hydrological loading (HYDL).

Figure 12 shows the correlations between the displacement time series and the NT-L models in the CM-frame, which are all positive. Figure 13 shows the RMS differences between the site displacements and the NT-L models. For the N component, the RMS differences are generally higher than for the E component (0.40 cm as against 0.26 cm on average), especially in equatorial regions. This can mainly be related to the less stable determination

Table 8
Datum Parameters of the Combined Solutions With Respect to ITRF2014. In Addition, Δ Denotes the Improvement of the WRMS of the F-ERF Solution Compared to the U-ERF Solution

| Technique	Datum parameter	U-ERF Wmean [mm]	U-ERF WRMS [mm]	F-ERF Wmean [mm]	F-ERF WRMS [mm]	Δ [%]
SLR	t_x	−1.6	3.9	−1.1	3.3	−17
	t_y	−0.1	3.3	−0.4	2.7	−19
	t_z	1.5	7.1	1.2	5.4	−24
	scale	1.4	3.0	1.4	2.5	−18
VLBI	t_x	−0.6	4.5	−0.1	3.2	−29
	t_y	3.5	4.1	2.0	3.4	−17
	t_z	1.2	6.1	0.6	4.3	−30
	scale	3.4	3.6	3.5	2.9	−20
GNSS	t_x	0.0	3.5	0.6	2.7	−21
	t_y	0.9	3.1	0.7	2.3	−26
	t_z	−2.0	6.0	−1.7	4.3	−28
	scale	3.3	3.0	2.4	2.6	−15

of the origin of the *z*-coordinate of the reference frame (cf. Figure 9) and confirms a good agreement although the correlations for regions with a small effect are reduced due to the higher short-term variations of both the station displacement and the modeled NT-L time series in the CM-frame. The largest RMS differences occur for the Up (U) component with an average of 0.62 cm and maximum values >1 cm for time series in hydrologically active regions like the Amazon basin (such as for the NAUS site).

Figure 14 shows the displacement time series for the sites discussed in Section 2. The F-ERF solution, in contrast to the SIRGAS-repro solution (cf. Figure 3), resembles the NT-L model relating to the CM-frame rather than that relating to the CF-frame. This is reaffirmed by investigating the correlation coefficients between the SIRGAS-repro and F-ERF solutions and the NT-L model displacements in CM-frame and CF-frame (cf. Table 10): While the SIRGAS-repro solution correlates well with the NT-L model displacements in CF-frame, it does not represent the displacements in CM-frame. This holds especially for the N and E components where the displacements are rather small. The F-ERF solution, on the other hand, does not represent the NT-L model displacements in CF-frame but correlates with the displacements in CM-frame at a level comparable to that of the SIRGAS-repro solution in CF-frame. A reduced quality is visible mainly for the U components of RIO2 and PALM, which is due to the fact that the NT-L displacements are small and that unmodeled geophysical effects together with remaining inaccuracies in the z-component of the realized origin (larger scatter as compared to the x- and y-component, cf. Figure 8) decrease the accuracy of the U component of stations in high southern latitudes. The effect is also visible in the N components of BELE and NAUS, the stations close to the equator, but less significant due to larger NT-L displacements. For NAUS, a disagreement is visible in the E component
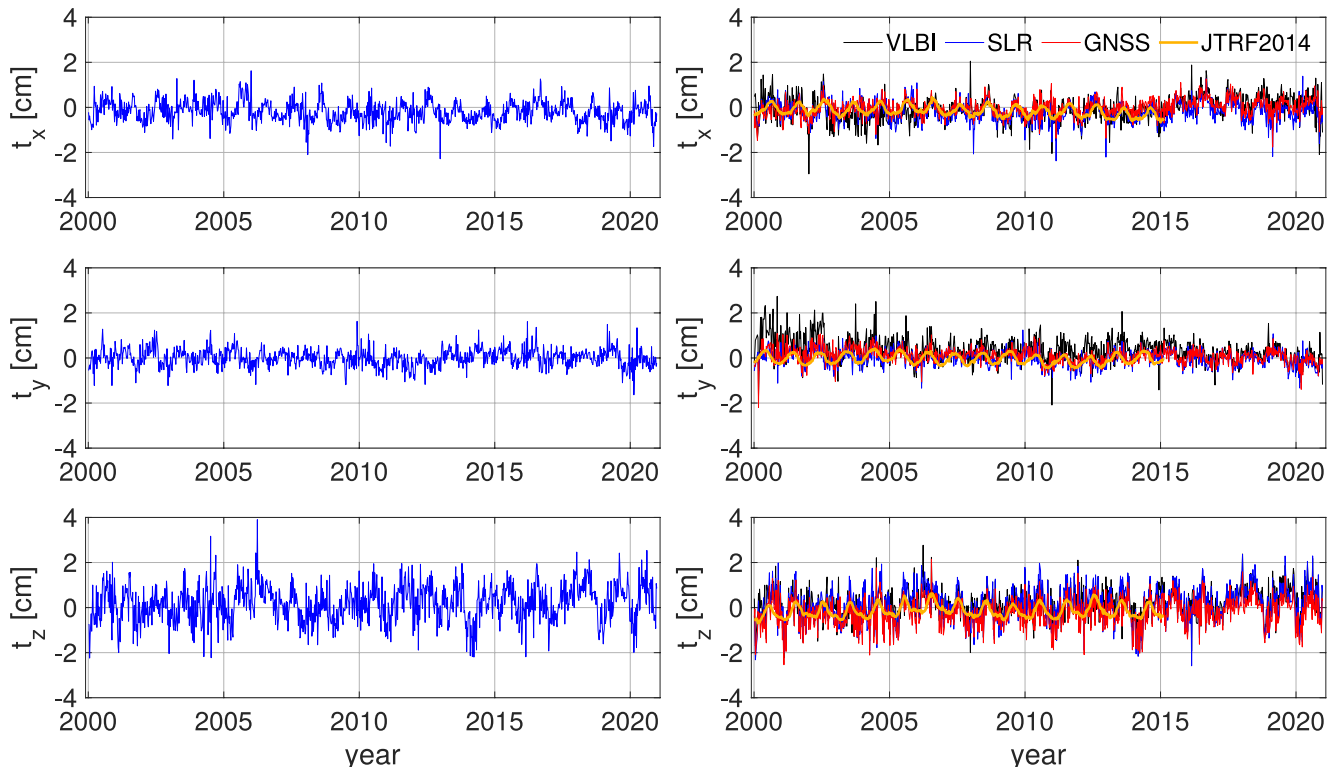
Figure 8. Translations with respect to ITRF2014 of the SLR single-technique solution (left) as well as of the technique-specific subnetworks of the U-ERF solution and of the GNSS subnetwork of the JTRF2014 (right).
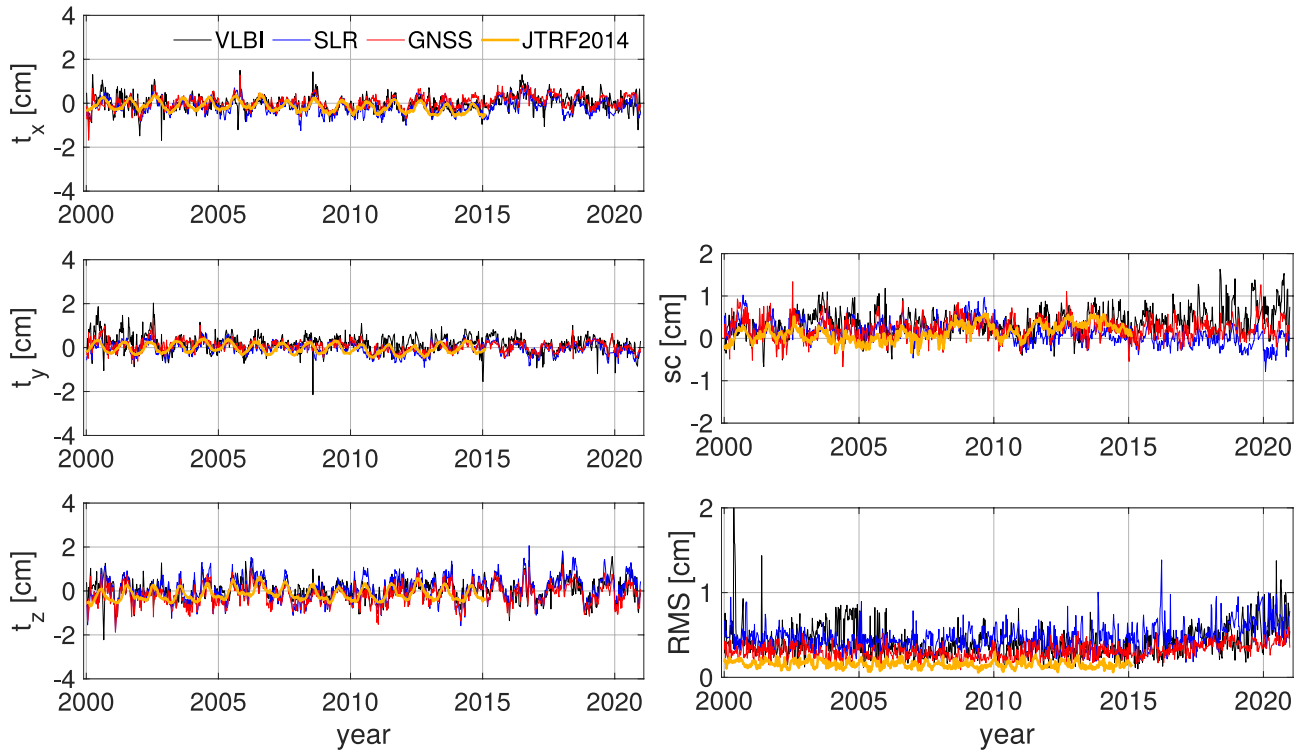
Figure 9. Translations (left), scale difference and RMS of the residuals of the Helmert transformation (right) of the F-ERF solution and of the JTRF2014 with respect to ITRF2014.
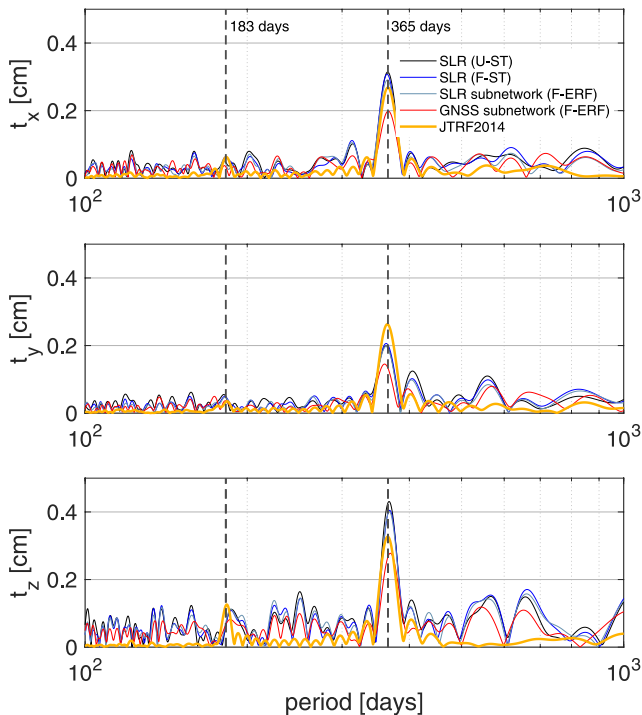
Figure 10. Spectra of the translation time series with respect to ITRF2014 of (a) the SLR U-ST solution, (b) the SLR F-ST solution, (c) the SLR subnetwork of the combined F-ERF solution, (d) the GNSS subnetwork of the combined F-ERF solution, and (e) the GNSS subnetwork of the JTRF2014.

between the NT-L time series provided by ESMGFZ and the observed site displacement time series, for both the SIRGAS-repro and F-ERF solutions (Figure 14). The effect might thus be related to model assumptions for the hydrological conditions causing the Earth's elastic deformation response in the hydrologically active Amazon basin (e.g., Martens et al., 2016), as the station is located close to the confluence of multiple rivers.

7. Conclusions and Outlook

The paper presents series of weekly regional ERFs for Latin America (SIRGAS network) with a direct geocentric datum realization by combining global GNSS, SLR, and VLBI networks. By implementing a filter method for the techniques SLR and VLBI, which are essential for the realization of the origin and the scale, we could significantly improve the stability of the epoch-wise independent datum realization. Compared to the unfiltered solution, the WRMS deviation, or the scatter, of the realized epoch-wise origins of the regional GNSS network with respect to the ITRF2014 origin could be reduced by 21%, 26%, and 28% in the *x*-, *y*-, and z-component, respectively. This confirms the benefits of the filtering approach and the importance of stable observational networks for realizing geocentric ERFs.

Our approach is based on geodetic standard products currently available for VLBI and GNSS. In the case of SLR, the ILRS 5-satellite setup extended by LARES has been used, which will become the routinely processed ILRS constellation in the near future. As global networks serve to realize the datum, the combination strategy is not dominantly dependent on co-location sites (or, in the classical sense, fiducial stations) in the region of interest.

Table 9
Datum Parameters of the F-ERF Solution With Respect to JTRF2014 Computed for the GNSS Subnetwork
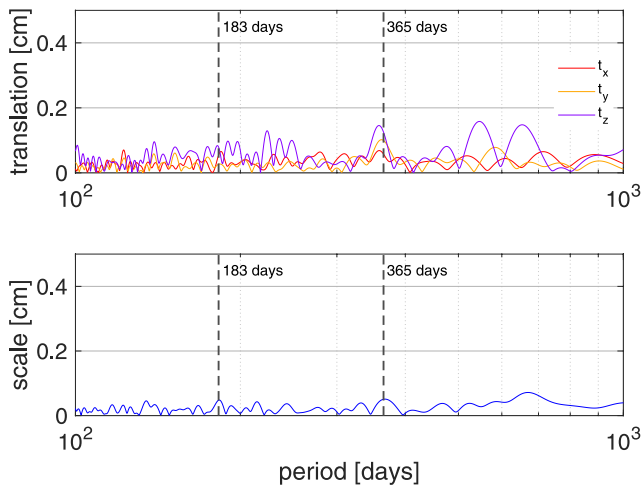
Datum parameter	Wmean [mm]	WRMS [mm]
t_x	1.0	3.1
t_y	0.3	3.0
t_z	−0.7	4.6
Scale	1.8	2.2

As long as a sufficient number of globally well-distributed co-location sites with measured local ties is available, the datum can be realized in a reliable way. Thus, the developed approach is conceptually transferable to any other region, independent of the number of locally available co-location sites.

The consequence of our approach chosen for the filtering and the introduction of the local ties is that the physical datum parameters origin and scale are realized directly from observations made within a limited time span of a few weeks. With the exception of the orientation, the approach thus avoids aligning the datum to potentially inaccurate linearly extrapolated reference coordinates. As the filtering is applied to the technique-specific NEQs before the combination, each combined solution realizes an independent datum that is transferred between the technique-specific networks via automatically selected and weighted local ties. The advantage of this approach is that each epoch-wise ERF realization can be computed independently from its predecessors (using the most recent weeks of observation data). This treatment is a consequence of our goal to enable an epoch-wise realization of the ERF at short latencies (up to a couple of weeks). It is in contrast with other approaches like that of the JTRF2014 (Abbondanza et al., 2017) where local ties are introduced at their measurement epoch and transferred forwards and backwards in time via co-motion constraints. Thereby, station position variations must be explicitly modeled, while the filtering of all networks over the whole observation time span requires a high computational effort but delivers highly accurate position time series for all stations in the contributing networks.

The implemented combination methodology has demonstrated the capability of the filtering approach for bridging observational gaps particularly for the SLR and VLBI networks. Comparisons with geophysical loading models reaffirm that our solution reflects both local effects and the so-called geocenter variations and is thus suitable for a direct interpretation with respect to geophysical effects in a global context. Despite this, only a further increase in station performances and availabilities, as recommended by various studies based on network and simulation analyses, will allow us to further improve the accuracy and temporal resolution of low-latency ERFs as short-term realizations of the ITRS. Especially the origin of the z-coordinate of the ERFs can potentially be improved in the near future by including more SLR satellites in highly inclined orbits and additional SLR sites in near-polar regions in the solution. Another limiting factor for the datum transfer between the techniques is currently the non-standardized provision of local tie measurements, which may lead to the problem of losing valid local tie values in regions of high seismic activity. We consider it important that local ties be remeasured and published regularly so that all local tie constellations are available with up-to-date values.

The approach to directly realize a geocentric datum for the regional network helps to provide a reference to monitor the impacts of earthquakes, natural hazards, and global change in specific areas. Being geocentric at all epochs—thus, relating to the defined origin of the Earth system—the solutions may help to integrate different geodetic and geophysical observation types into one common system, which might be a crucial contribution to enable long-term and short-latency analysis of geophysically induced phenomena in the context of the Global Geodetic Observing System (GGOS; Plag & Pearlman, 2009). In this way, our approach can be a valuable complement to the existing highly accurate secular and sub-secular multi-year realizations of the ITRS, which—for processing reasons—always include a closed observation time span and are realized at intervals of several years. Our approach, on the other hand, is rather designed for an operational use. Our concept of filtering recent data of the datum-relevant techniques over a limited time span and the strategy for automatic selection and introduction of local ties allows us to realize an epoch-wise geocentric datum with homogeneous accuracy over time. Future evolution of the observing networks will help to reduce remaining deficiencies due to remaining network effects or changing local tie constellations.
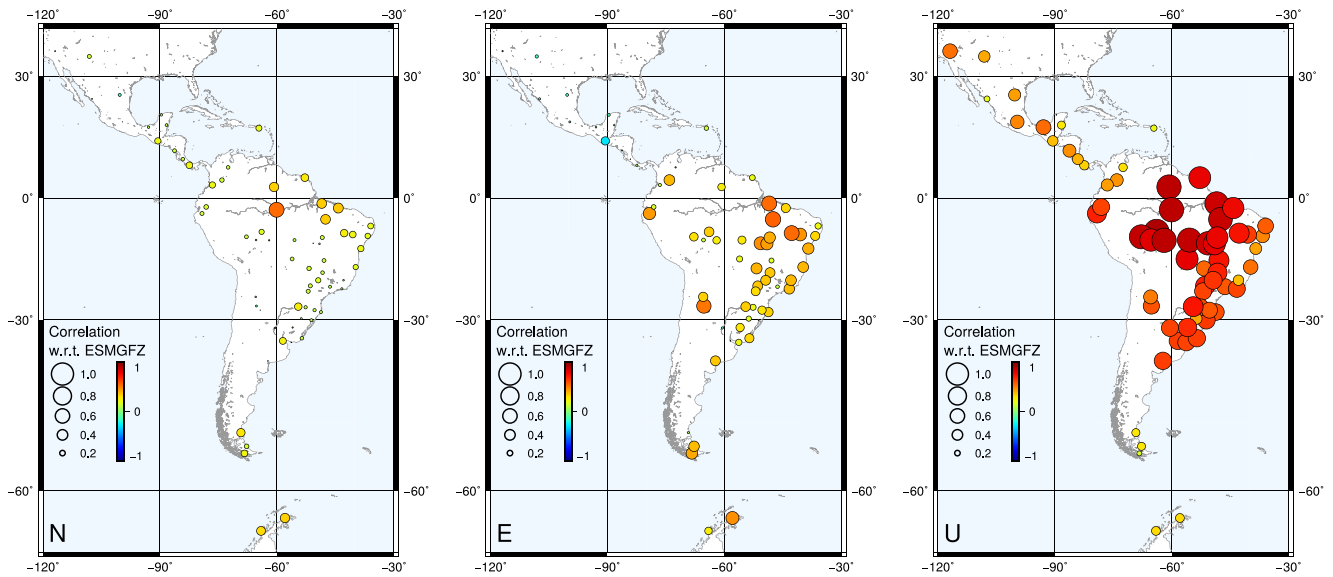

Figure 11. Spectra of the translation and scale offset time series of the GNSS subnetwork of the F-ERF solution with respect to JTRF2014.

Figure 12. Correlations between the site displacement time series derived from the F-ERF solution and the ESMGFZ NT-L time series in CM-frame.
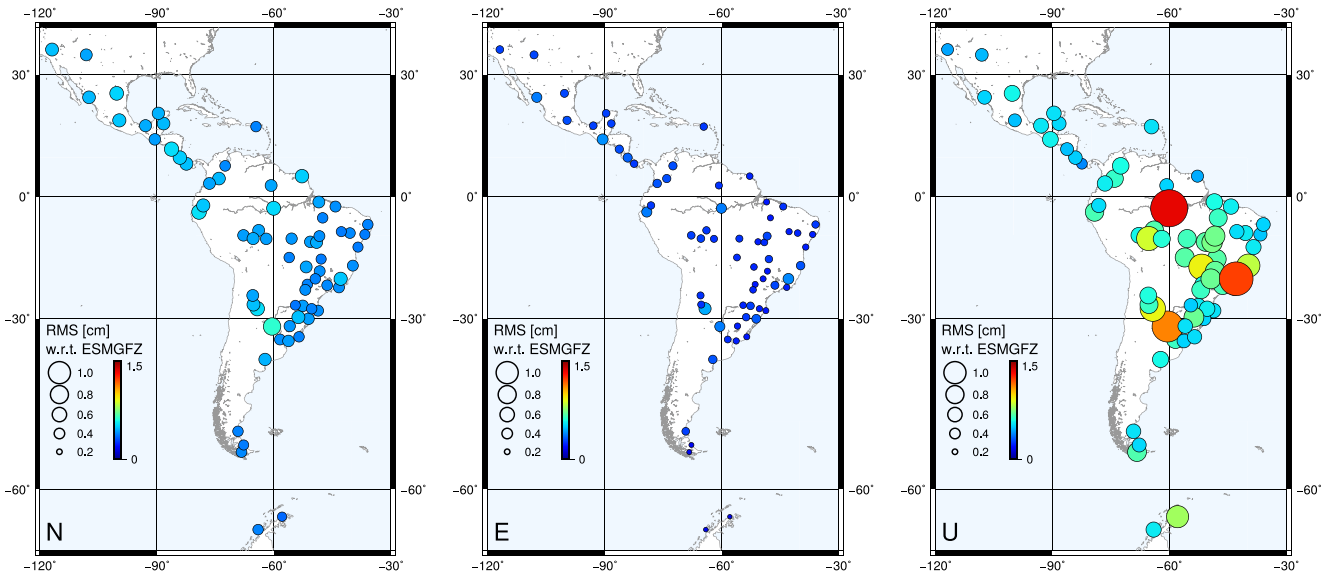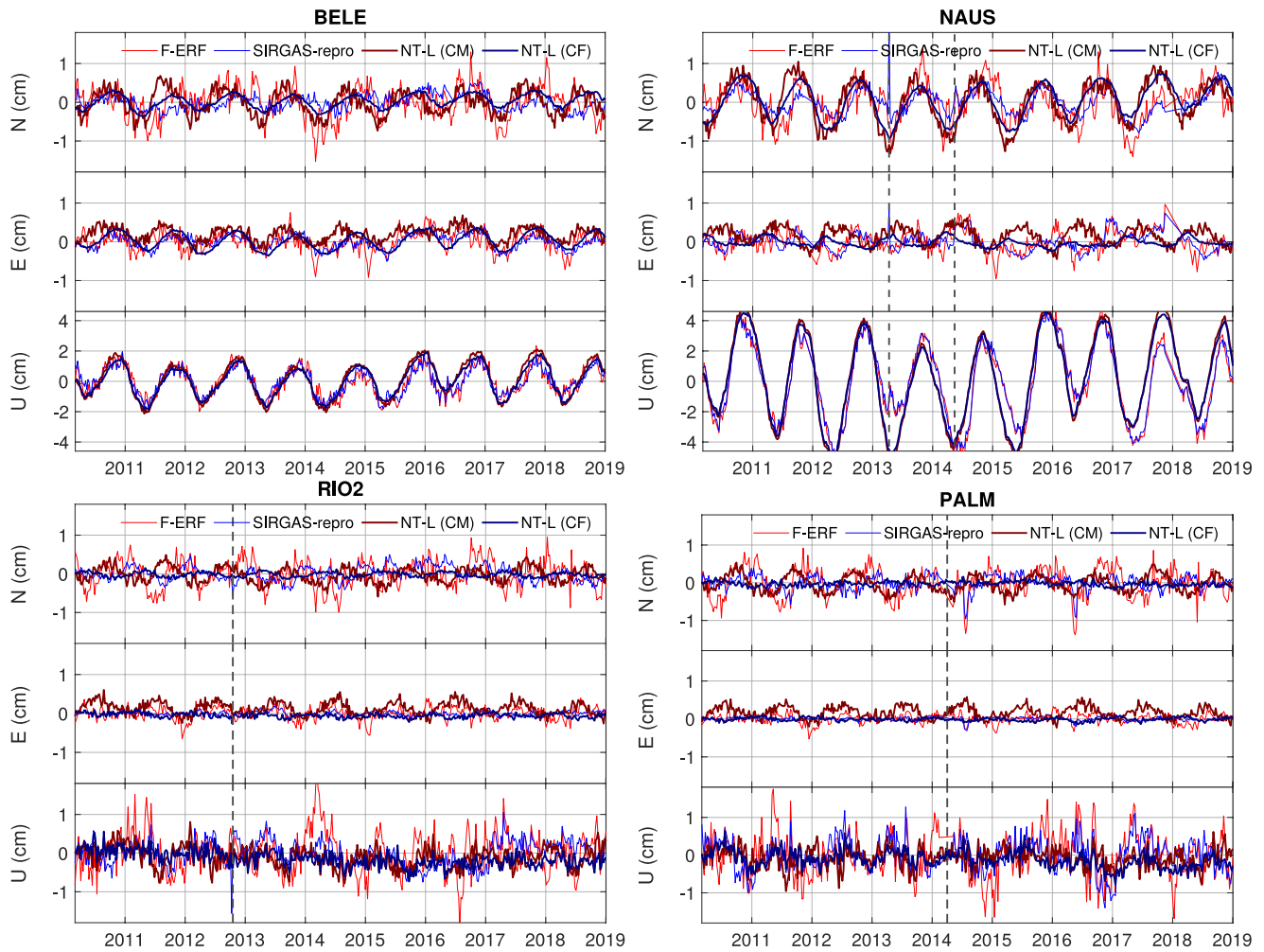

Figure 13. RMS difference between the site displacement time series derived from the F-ERF solution and the ESMGFZ NT-L time series in CM-frame.

Figure 14. Coordinate time series of stations BELE, NAUS, RIO2, and PALM from the F-ERF solution compared with the ESMGFZ NT-L time series in CM- and CF-frame (cf. Figure 3).

Table 10
Correlation Coefficients Between the N, E, and U Displacement Time Series Derived From the SIRGAS-Repro and F-ERF Solutions, Respectively, and the NT-L Models in CM- and CF-Frames

Station	NT-L Frame	SIRGAS-repro ρ_N	ρ_E	ρ_U	F-ERF solution ρ_N	ρ_E	ρ_U
BELE	CM	*0.0*	*0.4*	*0.9*	0.4	0.6	0.9
	CF	0.4	0.7	0.9	*0.4*	*0.5*	*0.9*
NAUS	CM	*0.4*	*−0.3*	*0.9*	0.6	−0.1	0.9
	CF	0.6	0.0	0.9	*0.6*	*−0.1*	*0.9*
RIO2	CM	*−0.5*	*0.0*	*0.1*	0.2	0.4	0.3
	CF	0.4	0.3	0.4	*−0.4*	*−0.1*	*0.2*
PALM	CM	*−0.3*	*−0.4*	*0.2*	0.3	0.3	0.3
	CF	0.0	0.3	0.6	*−0.3*	*−0.2*	*0.3*

Note. Roman numbers refer to the comparison considered consistent (SIRGAS-repro against CF-related NT-L time series and F-ERF solution against CM-related NT-L time series), italicized numbers refer to the cross-comparison.

Data Availability Statement

All data processed within this study are publicly available. SLR observation data are provided by the International Laser Ranging Service (ILRS) and have been accessed via the EUROLAS Data Centre hosted at DGFI-TUM (EDC, https://edc.dg/fi.tum.de/en/; last access: 2021-08-11). VLBI data are provided by the International VLBI Service for Geodesy and Astrometry (IVS) and have been accessed via NASA's Crustal Dynamics Data Information System (CDDIS, https://cddis.nasa.gov; last access: 2021-08-11). GNSS data of the global IGS stations are provided by the International GNSS Service (IGS) via NASA's CDDIS. The GNSS data of the SIRGAS stations are provided by the SIRGAS Data Centres (https://sirgas.ipgh.org/en/gnss-network/data-centres/). The GNSS data reprocessed for this study are available from the IGS Regional Network Associate Analysis Centre for SIRGAS hosted at DGFI-TUM (ftp.SIRGAS.org/pub/gps/SIRGAS/REPRO2/).

References

Abbondanza, C., Chin, T. M., Gross, R. S., Heflin, M. B., Parker, J. W., Soja, B. S., et al. (2017). JTRF2014, the JPL Kalman filter and smoother realization of the International Terrestrial Reference System. *Journal of Geophysical Research: Solid Earth*, *122*(10), 8474–8510. https://doi.org/10.1002/2017JB014360

Abbondanza, C., Chin, T. M., Gross, R. S., Heflin, M. B., Parker, J. W., Soja, B. S., & Wu, X. (2020). A sequential estimation approach to terrestrial reference frame determination. *Advances in Space Research*, *65*(4), 1235–1249. https://doi.org/10.1016/j.asr.2019.11.016

Altamimi, Z. (2018). *EUREF Technical Note 1: Relationship and Transformation between the International and the European Terrestrial Reference Systems (Tech. Rep.)*. Institut National de l'Information Géographique et Forestière (IGN). Retrieved 2022-06-15, from http://etrs89.ensg.ign.fr/pub/EUREF-TN-1.pdf

Altamimi, Z., Rebischung, P., Métivier, L., & Collilieux, X. (2016). ITRF2014: A new release of the International Terrestrial Reference Frame modeling nonlinear station motions. *Journal of Geophysical Research: Solid Earth*, *121*(8), 6109–6131. https://doi.org/10.1002/2016JB013098

Angermann, D., Drewes, H., Krügel, M., Meisel, B., Gerstl, M., Kelm, R., et al. (2004). *ITRS combination center at DGFI: A Terrestrial Reference Frame Realization 2003*. München (Munich), Germany: Deutsche Geodätische Kommission (DGK) Reihe B, 313. Verlag der Bayerischen Akademie der Wissenschaften in Kommission beim Verlag C. H. Beck.

Assimakis, N., Adam, M., & Douladiris, A. (2012). Information Filter and Kalman Filter Comparison: Selection of the Faster Filter. *International Journal of Information Engineering*, *2*(1), 1–5.

Bevis, M., Alsdorf, D., Kendrick, E., Fortes, L. P., Forsberg, B., Smalley, R., Jr., & Becker, J. (2005). Seasonal fluctuations in the mass of the Amazon River system and Earth's elastic response. *Geophysical Research Letters*, *32*(16), L16308. https://doi.org/10.1029/2005GL023491

Blewitt, G., Lavallée, D., Clarke, P., & Nurutdinov, K. (2001). A new global mode of Earth deformation: Seasonal cycle detected. *Science*, *294*(5550), 2342–2345. https://doi.org/10.1126/science.1065328

Bloßfeld, M. (2015). *The key role of Satellite Laser Ranging towards the integrated estimation of geometry, rotation and gravitational field of the Earth* (p. 745). Deutsche Geodätische Kommission (DGK) Reihe C.

Bloßfeld, M., & Kehm, A. (2020). *ILRS analysis activities. DGFI-TUM (Deutsches Geodätisches Forschungsinstitut – Technische Universität München), Germany*. In C. Noll, & M. Pearlman (Eds.), *International Laser Ranging Service 2016–2019 Report NASA/TP-20205008530* (pp. 710–713). Greenbelt, MD: National Aeronautics and Space Administration, Goddard Space Flight Center.

Bloßfeld, M., Rudenko, S., Kehm, A., Panafidina, N., Müller, H., Angermann, D., et al. (2018). Consistent estimation of geodetic parameters from SLR satellite constellation measurements. *Journal of Geodesy*, *92*(9), 1003–1021. https://doi.org/10.1007/s00190-018-1166-7

Bloßfeld, M., Seitz, M., & Angermann, D. (2014). Non-linear station motions in epoch and multi-year reference frames. *Journal of Geodesy*, *88*(1), 45–63. https://doi.org/10.1007/s00190-013-0668-6

Bloßfeld, M., Seitz, M., & Angermann, D. (2015). *Epoch reference frames as short-term realizations of the ITRS. Datum stability versus sampling*. In C. Rizos, & P. Willis (Eds.), *IAG 150 Years. IAG Symposia* (Vol. *143*, pp. 27–32). Springer. https://doi.org/10.1007/1345_2015_91

Brunini, C., Sánchez, L., Drewes, H., Costa, S., Mackern, V., Martínez, W., et al. (2012). Improved analysis strategy and accessibility of the SIRGAS Reference Frame. In S. Kenyon, M. Pacino, & U. Marti (Eds.), *Geodesy for Planet Earth. IAG Symposia* (Vol. 136, pp. 3–10). Springer. https://doi.org/10.1007/978-3-642-20338-1_1

Chin, T. (2001). On Kalman filter solution of space-time interpolation. *IEEE Transactions on Image Processing*, *10*(4), 663–666. https://doi.org/10.1109/83.913601

Chin, T. (2020). Realization of time sequential estimation of terrestrial reference frame using square-root information filter and smoother. *Paper presented at the European Geosciences Union General Assembly 2020, EGU2020-10805*. https://doi.org/10.5194/egusphere-egu2020-10805

Collilieux, X., & Altamimi, Z. (2009). *Impact of the network effect on the origin and scale: Case study of satellite laser ranging*. In M. G. Sideris (Ed.), *Observing our Changing Earth. Proceedings of the 2007 IAG General Assembly*. (pp. 31–37). Perugia, Italy: Springer.

Collilieux, X., Altamimi, Z., Coulot, D., van Dam, T., & Ray, J. (2010). Impact of loading effects on determination of the International Terrestrial Reference Frame. *Advances in Space Research*, 4*5*(1), 144–154. https://doi.org/10.1016/j.asr.2009.08.024

Collilieux, X., Altamimi, Z., Ray, J., van Dam, T., & Wu, X. (2009). Effect of the satellite laser ranging network distribution on geocenter motion estimation. *Journal of Geophysical Research: Solid Earth,* 1*14*(B4), B04402. https://doi.org/10.1029/2008JB005727

Collilieux, X., van Dam, T., Ray, J., Coulot, D., Métivier, L., & Altamimi, Z. (2012). Strategies to mitigate aliasing of loading signals while estimating GPS frame parameters. *Journal of Geodesy*, 8*6*(1), 1–14. https://doi.org/10.1007/s00190-011-0487-6

Dach, R., Lutz, S., Walser, P., & Fridez, P. (2015). *Bernese GNSS software version 5.2 (Tech. Rep.)*. Berne, Switzerland: Astronomical Institute, University of Bern.

Dill, R., & Dobslaw, H. (2013). Numerical simulations of global-scale high-resolution hydrological crustal deformations. *Journal of Geophysical Research: Solid Earth*, *118*(9), 5008–5017. https://doi.org/10.1002/jgrb.50353

Dong, D., Yunck, T., & Heflin, M. (2003). Origin of the International Terrestrial Reference Frame. *Journal of Geophysical Research: Solid Earth*, *108*(B4), 2200. https://doi.org/10.1029/2002JB002035

Drewes, H. (2009). The actual plate kinematic and crustal deformation model APKIM2005 as basis for a non-rotating ITRF. In H. Drewes (Ed.), *Geodetic Reference Frames. IAG Symposia* (Vol. 134, pp. 95–99). Springer. https://doi.org/10.1007/978-3-642-00860-3_15

Drewes, H., Angermann, D., & Seitz, M. (2013). Alternative definitions of the terrestrial reference system and its realization in reference frames. In *Reference frames for applications in geosciences* (pp. 39–44). Springer. https://doi.org/10.1007/978-3-642-32998-2_7

Drewes, H., Kaniuth, K., Vö1ksen, C., Costa, S. M. A., & Fortes, L. P. S. (2005). Results of the SIRGAS campaign 2000 and coordinates variations with respect to the 1995 South American geocentric reference frame. In *A Window on the Future of Geodesy* (pp. 32–37). Springer. https://doi.org/10.1007/3-540-27432-4_6

Gauss, C. F. (1823). *Theoria combinationis observationum erroribus minimis obnoxiae*. In *Commentationes Societatis Regiae Scientiarum Gottingensis Recentiores – Classis Physicae* (Vol. 5, pp. 33–90). Gottingae (Göttingen), Kingdom of Hanover: Henricus Dieterich.

Gerstl, M. (1997). Parameterschätzung in DOGS-OC. In *DGFI Interner Bericht MG/01/1996/DGFI, 2. Auflage (Tech. Rep.)*. Munich, Germany: Deutsches Geodätisches Forschungsinstitut (DGFI).

Gerstl, M., Kelm, R., Müller, H., & Ehrnsperger, W. (2008). DOGS-CS – Kombination und Lösung großer Gleichungssysteme. In *DGFI Interner Bericht MG/01/1995/DGFI, Version 01.10.2008 (Tech. Rep.)*. Munich, Germany: Deutsches Geodätisches Forschungsinstitut (DGFI).

Glaser, S., König, R., Ampatzidis, D., Nilsson, T., Heinkelmann, R., Flechtner, F., & Schuh, H. (2017). A Global Terrestrial Reference Frame from simulated VLBI and SLR data in view of GGOS. *Journal of Geodesy*, *91*(7), 723–733. https://doi.org/10.1007/s00190-017-1021-2

Glaser, S., König, R., Neumayer, K. H., Balidakis, K., & Schuh, H. (2019). Future SLR station networks in the framework of simulated multi-technique terrestrial reference frames. *Journal of Geodesy*, *93*(11), 2275–2291. https://doi.org/10.1007/s00190-019-01256-8

Glaser, S., König, R., Neumayer, K. H., Nilsson, T., Heinkelmann, R., Flechtner, F., & Schuh, H. (2019). On the impact of local ties on the datum realization of global terrestrial reference frames. *Journal of Geodesy*, *93*(5), 655–667. https://doi.org/10.1007/s00190-018-1189-0

Glomsda, M., Bloßfeld, M., Seitz, M., & Seitz, F. (2021). Correcting for site displacements at different levels of the Gauss-Markov model – A case study for geodetic VLBI. *Advances in Space Research*, *68*(4), 1645–1662. https://doi.org/10.1016/j.asr.2021.04.006

Glomsda, M., Seitz, M., Angermann, D., & Gerstl, M. (2021). DGFI-TUM analysis center Biennial Report 2019+2020. In D. Behrend, K. L. Armstrong, & K. D. Baver (Eds.), *International VLBI Service for Geodesy and Astrometry 2019+2020 Biennial Report NASA/TP–20210021389* (pp. 201–205). Greenbelt, MD: National Aeronautics and Space Administration, Goddard Space Flight Center.

Glomsda, M., Seitz, M., Gerstl, M., Kehm, A., Bloßfeld, M., & Angermann, D. (2020). Impact of new models for the ITRF2020 in VLBI analysis at DGFI-TUM. *Paper presented at the AGU Fall Meeting 2020*. Retrieved 2022-06-15, from https://mediatum.ub.tum.de/?id=1586328

Gómez, D. D., Bevis, M. G., & Caccamise, D. J., II. (2022). Maximizing the consistency between regional and global reference frames utilizing inheritance of seasonal displacement parameters. *Journal of Geodesy*, *96*, 9. https://doi.org/10.1007/s00190-022-01594-0

Johnston, G., Riddell, A., & Hausler, G. (2017). The International GNSS Service. In P. J. G. Teunissen, & O. Montenbruck (Eds.), *Springer handbook of global navigation satellite systems* (pp. 967–982). Springer. https://doi.org/10.1007/978-3-319-42928-1_33

Kalman, R. E. (1960). A new approach to linear filtering and prediction problems. *Transactions of the ASME–Journal of Basic Engineering*, *82*, 35–45. https://doi.org/10.1115/1.3662552

Kehm, A., Bloßfeld, M., König, P., & Seitz, F. (2019). Future TRFs and GGOS—Where to put the next SLR station? *Advances in Geosciences*, *50*, 17–25. https://doi.org/10.5194/adgeo-50-17-2019

Kehm, A., Bloßfeld, M., Pavlis, E. C., & Seitz, F. (2018). Future global SLR network evolution and its impact on the terrestrial reference frame. *Journal of Geodesy*, *92*(6), 625–635. https://doi.org/10.1007/s00190-017-1083-1

Koch, K.-R. (2004). *Parameterschätzung und Hypothesentests in linearen Modellen. Vierte, bearbeitete Auflage*. Bonn, Germany: Ehemals Ferd. Dümmlers Verlag. Retrieved 2022-06-15, from http://www.geod.uni-bonn.de

Kouba, J. (2009). A guide to using International GNSS Service products. Retrieved 2022-06-15, from https://www.igs.org/wp-content/uploads/2019/08/UsingIGSProductsVer21_cor.pdf

Kwak, Y., Gerstl, M., Bloßfeld, M., Angermann, D., Schmid, R., & Seitz, M. (2017). DOGS-RI: New VLBI analysis software at DGFI-TUM. In R. Haas, & G. Elgered (Eds.), *Proceedings of the 23rd European VLBI Group for Geodesy and Astrometry Working Meeting* (pp. 212–215). Chalmers.

Martens, H. R., Simons, M., Owen, S., & Rivera, L. (2016). Observations of ocean tidal load response in South America from subdaily GPS positions. *Geophysical Journal International*, *205*(3), 1637–1664. https://doi.org/10.1093/gji/ggw087

Nothnagel, A., Artz, T., Behrend, D., & Malkin, Z. (2017). International VLBI service for geodesy and astrometry – Delivering high-quality products and embarking on observations of the next generation. *Journal of Geodesy*, *91*(7), 711–721. https://doi.org/10.1007/s00190-016-0950-5

Otsubo, T., Matsuo, K., Aoyama, Y., Yamamoto, K., Hobiger, T., Kubo-oka, T., & Sekido, M. (2016). Effective expansion of satellite laser ranging network to improve global geodetic parameters. *Earth Planets and Space*, *68*(1), 1–7. https://doi.org/10.1186/s40623-016-0447-8

Pavlis, E. C., & Kuźmicz-Cieślak, M. (2009). SLR and the next generation global geodetic networks. In S. Schillack, (Ed.), *Proceedings of the 16th International Workshop on Laser Ranging*. Retrieved 2022-06-15, from https://cddis.nasa.gov/lw16/docs/papers/ggo_5_Pavlis_p.pdf

Pearlman, M. R., Noll, C. E., Pavlis, E. C., Lemoine, F. G., Combrink, L., Degnan, J. J., et al. (2019). The ILRS: Approaching 20 years and planning for the future. *Journal of Geodesy*, *93*(11), 2161–2180. https://doi.org/10.1007/s00190-019-01241-1

Petit, G., & Luzum, B. (2010). *IERS conventions (2010). IERS Technical Note 36, v 1.3.0 (Tech. Rep.)*. Frankfurt am Main, Germany: International Earth Rotation and Reference Systems Service.

Plag, H.-P., & Pearlman, M. (Eds.). (2009). *Global Geodetic Observing System*. Berlin, Germany: Springer.

Ray, J., Altamimi, Z., Collilieux, X., & van Dam, T. (2008). Anomalous harmonics in the spectra of GPS position estimates. *GPS Solutions*, *12*(1), 55–64. https://doi.org/10.1007/s10291-007-0067-7

Rebischung, P. (2020). Switch to IGb14 reference frame [IGSMAIL-7921]. Retrieved 2022-06-15, from https://lists.igs.org/pipermail/igsmail/2020/007917.html

Rebischung, P., & Schmid, R. (2016). *IGS14/igs14.atx: A new framework for the IGS products*. AGU Fall Meeting 2016. Abstract G41A-0998. San Francisco, CA.

Rebischung, P., Schmid, R., & Herring, T. (2016). Upcoming switch to IGS14/igs14. atx [IGSMAIL-7399]. Retrieved 2022-06-15, from https://lists.igs.org/pipermail/igsmail/2016/001233.html

Sánchez, L., & Drewes, H. (2016). Crustal deformation and surface kinematics after the 2010 earthquakes in Latin America. *Journal of Geodynamics*, *102*, 1–23. https://doi.org/10.1016/j.jog.2016.06.005

Sánchez, L., & Drewes, H. (2020). Geodetic monitoring of the variable surface deformation in Latin America. In J. Freymueller, & L. Sánchez (Eds.), *IAG Symposia* (Vol. *152*). https://doi.org/10.1007/1345_2020_91

Sánchez, L., Drewes, H., Brunini, C., Mackern, M., & Martínez-Díaz, W. (2016). SIRGAS core network stability. In C. Rizos, & P. Willis (Eds.), *IAG 150 Years. IAG Symposia*, (Vol. 143, pp. 183–191). Springer. https://doi.org/10.1007/1345_2015_143

Sánchez, L., Drewes, H., Kehm, A., & Seitz, M. (2022). SIRGAS reference frame analysis at DGFI-TUM. *Journal of Geodetic Science*. (in press).

Sánchez, L., & Kehm, A. (2021). SIRGAS regional network associate analysis centre (IGS RNAAC SIRGAS) (Technical Report). In A. Villiger, & R. Dach (Eds.), *International GNSS service technical report 2020 (IGS annual report)* (pp. 135–146). IGS Central Bureau and University of Bern; Bern Open Publishing. https://doi.org/10.48350/156425

Sánchez, L., Seemüller, W., Drewes, H., Mateo, L., González, G., Da Silva, A., et al. (2013). Long-term stability of the SIRGAS reference frame and episodic station movements caused by the seismic activity in the SIRGAS region. In Z. Altamimi, & X. Collilieux (Eds.), *Reference Frames for Applications in Geosciences. IAG Symposia* (Vol. 138, pp. 153–161). Springer. https://doi.org/10.1007/978-3-642-32998-2_24

Schön, S., & Brunner, F. K. (2008). A proposal for modelling physical correlations of GPS phase observations. *Journal of Geodesy*, *82*(10), 601–612. https://doi.org/10.1007/s00190-008-0211-3

Schön, S., & Kutterer, H. (2007). A comparative analysis of uncertainty modelling in GPS data analysis. In P. Tregoning, & R. Rizos (Eds.), *Dynamic Planet: Monitoring and Understanding a Dynamic Planet with Geodetic and Oceanographic Tools*. *IAG Symposia* (Vol. 130, pp. 137–142). https://doi.org/10.1007/978-3-540-49350-1_22

Seitz, F., Hedman, K., Meyer, F. J., & Lee, H. (2014). Multi-sensor space observation of heavy flood and drought conditions in the Amazon region. In C. Rizos, & P. Willis (Eds.), *Earth on the Edge: Science for a Sustainable Planet*. *IAG Symposia* (Vol. 139, pp. 311–317). Springer. https://doi.org/10.1007/978-3-642-37222-3_41

Seitz, F., & Krügel, M. (2009). Inverse model approach for vertical load deformations in consideration of crustal inhomogeneities. In H. Drewes (Ed.), *Geodetic Reference Frames*. *IAG Symposia* (Vol. 134, pp. 23–29). Springer. https://doi.org/10.1007/978-3-642-00860-3_4

Seitz, M., Angermann, D., Bloßfeld, M., Drewes, H., & Gerstl, M. (2012). The 2008 DGFI realization of the ITRS: DTRF2008. *Journal of Geodesy*, *86*(12), 1097–1123. https://doi.org/10.1007/s00190-012-0567-2

Seitz, M., Angermann, D., Gerstl, M., Bloßfeld, M., Sánchez, L., & Seitz, F. (2015). Geometrical reference systems. In W. Freeden, M. Z. Nashed, & T. Sonar (Eds.), *Handbook of Geomathematics*. (2nd ed., pp. 1995–3034). Springer.

Seitz, M., Bloßfeld, M., Angermann, D., & Seitz, F. (2022). DTRF2014: DGFI-TUM's ITRS realization 2014. *Advances in Space Research*, *69*(6), 2391–2420. https://doi.org/10.1016/j.asr.2021.12.037

SIRGAS. (1997). SIRGAS final report; Working groups I and II IBGE. (Tech. Rep.). Retrieved from http://www.sirgas.org/fileadmin/docs/SIRGAS95RepEng.pdf

Willis, P., Lemoine, F. G., Moreaux, G., Soudarin, L., Ferrage, P., Ries, J., et al. (2015). The International DORIS Service (IDS): Recent developments in preparation for ITRF2013. In C. Rizos, & P. Willis (Eds.), *IAG 150 Years*. *IAG Symposia* (Vol. 143, pp. 631–640). Springer. https://doi.org/10.1007/1345_2015_164

Zou, R., Freymueller, J. T., Ding, K., Yang, S., & Wang, Q. (2014). Evaluating seasonal loading models and their impact on global and regional reference frame alignment. *Journal of Geophysical Research: Solid Earth*, *119*(2), 1337–1358. https://doi.org/10.1002/2013JB010186